SINGLE AND TWO PHASE CONTINUUM MODELING FOR LAMINAR FORCED CONVECTION OF NANOFLUIDS

by

Sinan Göktepe

B.S., Mechanical Engineering, Middle East Technical University

Northern Cyprus Campus, 2011

Submitted to the Institute for Graduate Studies in
Science and Engineering in partial fulfillment of
the requirements for the degree of
Master of Science

Graduate Program in Master of Science in Mechanical Engineering

Boğaziçi University

2013

SINGLE AND TWO PHASE CONTINUUM MODELING FOR LAMINAR FORCED CONVECTION OF NANOFLUIDS

APPROVED BY:

Assoc. Prof. Kunt Atalık .....
(Thesis Supervisor)

Assoc. Prof. Hakan Ertürk .....
(Thesis Co-supervisor)

Assoc. Prof. Hasan Bedir .....

Prof. Akın Tezel .....

Prof. Ramazan Yıldırım .....

DATE OF APPROVAL: 06.06.2013

This thesis is dedicated to my parents Yeşim and Nuri Göktepe, my fiancée Müge Türegün, and to the memory my grandfather M. Kazım Göktepe

ACKNOWLEDGEMENTS

First and above all, I would like to express my sincere gratitude to my supervisor Assoc. Prof. Kunt Atalık and my co-supervisor Assoc. Prof. Hakan Ertürk for their invaluable guidance during my study. Despite of their busy schedule, they showed great effort and spared time for our discussions. I have experienced an excellent and unparalleled academic study under their supervision. I believe that, without their guidance this thesis would not be possible.

Second, I would also like to thank to the thesis committee for reviewing my manuscript and providing invaluable comments, despite their busy schedule.

My former professors in Middle East Technical University Northern Cyprus Campus have invaluable effort on me during my studies at METU NCC. I would like to thank them for all the knowledge and vision that they provided. Also, I would like to especially thank to Assist. Prof. Bülent Özer, Assist. Prof. Eray Uzgören, Prof. Orhan Yıldırım, and Prof. Rüknettin Oskay, for their support during my application to Boğaziçi University.

This thesis would not have been possible without the support of my parents, family, and especially my fiancée Müge. I am grateful to them for their never-ending love, patience, encouragement and support.

Lastly, I would like to thank to TÜBİTAK for its financial support during my academic study under the grant 111M1777 of the 1001 Program.

ABSTRACT

SINGLE AND TWO PHASE CONTINUUM MODELING FOR LAMINAR FORCED CONVECTION OF NANOFLUIDS

Macroscopic modeling of nanofluids is necessary for design and analysis of equipment that rely on nanofluids. For the moment, there is no study that covers recent state-of-the-art nanofluid models, and compares their accuracy and computational efficiency. Single and two phase models have been investigated for the characterization of laminar forced convection of Al_2O_3-water nanofluid in a circular tube. Single-phase thermal dispersion model that uses velocity gradient, is found to be the most accurate single-phase model in prediction of convective heat transfer coefficient. Since, single-phase models fail in predicting pressure drop and friction factor, a new dispersion viscosity model is introduced for a better representation of effective nanofluid viscosity. In the study, Eulerian-Eulerian and Eulerian-Mixture models are also studied and it is found that they are under and over predicting heat transfer coefficient at entry and fully developed regions, respectively. Considering its computational efficiency, Eulerian-Eulerian model is recommended for applications without calibration data, and if prediction of both heat transfer and pressure drop is important. For the first time, it is shown that the computational cost of Eulerian-Eulerian model can be reduced by the use of Full Multiphase Coupling algorithm. In the study, hexagonal boron nitride-water nanofluid is also studied, and results are compared with Al_2O_3-water nanofluid. Results indicate that non-granular assumption for two-phase models is questionable for highly thermally conductive particles.

ÖZET

NANOAKIŞKANLARIN KATMANLI ZORLANMIŞ KONVEKSİYONU İÇİN TEK VE İKİ FAZLI SÜREKLİ ORTAM MODELLEMESİ

Nanoakışklanların makroskopik modellenmesi, nanoakışkanlara dayalı ekipmanların tasarımı ve analizi için gereklidir. Şu an için, yeni ve üstün nanoakışkan modellerinin ve bu modellerin hesaplama verimliliklerinin karşılaştırıldığı bir çalışma literatürde bulunmamaktadır. Bu çalışmada, tek ve iki fazlı modeller ile Al_2O_3-su nano akışkanının boru içindeki katmanlı zorlanmış konveksiyonunun modellenmesi incelenmiştir. Hız gradyanı kullanılarak tanımlanan tek fazlı ısıl dağılım modelinin, ısı iletim katsayısını en doğru hesaplayan model olduğu gösterilmiştir. Tek fazlı modeller basınç düşüşünü doğru olarak öngöremediklerinden dolayı, bu modellerin nanoakışkanların hidrodinamik çözümlerindeki doğruluklarını arttırmak için, yeni bir dağılım viskozite modeli önerilmiştir. Bunlara ek olarak bu çalışmada, İki fazlı Euleryen-Euleryen ve Euleryen-Karışım modelleri incelenmiş ve modellerinin ısıl iletim katsayısını giriş bölgesinde düşük ve tam gelişmiş akış bölgesinde ise yüksek öngördüğü gözlemlenmiştir. Mevcut deneysel verinin olmadığı, ısıl iletim katsayısının ve akışın modellemesinin önemli olduğu durumlar için, hesaplama verimliliği de göz önünde bulundurularak Euleryen-Euleryen model tavsiye edilmiştir. Buna ek olarak, ilk kez Euleryen-Euleryen modelin hesaplama verimliliğinin Full Multiphase Coupled algoritması ile arttırılabileneceği gösterilmiştir. Son olarak ise, Hekzagonal Boron Nitrat–su nanoakışkanı incelenmiş ve sonuçları Al_2O_3-su nanoakışkanı ile karşılaştırılmıştır. Sonuçlar göstermektedir ki, iki fazlı modeller için granüler olmayan akış varsayımının geçerliliği yüksek ısıl iletkenliğe sahip parçacıklar için sorgulanabilir.

TABLE OF CONTENTS

LIST OF FIGURES

LIST OF TABLES

LIST OF SYMBOLS

$\vec{a}$	Acceleration of particles [m/s^2]
bf	Base fluid
br	Brownian
C_d	Drag coefficient in Eulerian-Eulerian model
col	Collision
d	Drag
c_p	Specific heat [J/kgK]
D	Diameter [m]
d_{bf}	Diameter of base fluid molecules [m]
$disp$	Dispersion
d_p	Particle diameter [m]
eff	Effective property
$\vec{F}$	Force vector
f_{app}	Apparent friction factor
f_d	Drag coefficient in Eulerian-Mixture model
f_x	Darcy friction coefficient
G	Particle-particle interaction modulus in Eulerian-Eulerian model
h_p	Particle heat transfer coefficient
h_v	Volumetric interphase heat transfer coefficient
h_x	Convective heat transfer coefficient
i	Enthalpy
k	Thermal conductivity [W/mK]
k_B	Boltzmann Constant [J/K]
L	Length [m]
m	Mixture
n	Shape factor
nf	Nanofluid
$\mathrm{Nu_x}$	Nusselt number

p	Particle
P	Pressure [Pa]
Pe	Peclet number
Pr	Prandtl number
r	Radial direction
R	Pipe radius [m]
Re	Reynolds number
T	Absolute temperature [K]
u, v	x and r velocity components [m/s]
U	Mean flow velocity
q''_{wall}	Wall convective heat flux [W/m^2]
$\vec{v}$	Velocity vector
$v_{dr,k}$	Drift velocity of phase k
vm	Virtual mass
x	Axial direction
x^*	Dimensionless axial distance for Equation 3.13
α	Thermal diffusivity [J/m^{3}K]
δ	Nanoparticle spacing [m]
λ	Mean free path [m]
μ	Viscosity [Pa $\cdot$ s]
ω	Geometry constant in Eulerian-Eulerian model
τ	Shear stress
φ	Volume fraction
ρ	Density [kg/m^3]
ζ	Eulerian-Eulerian model friction factor
$\parallel$	Parallel direction to the basal plane
$\perp$	Perpendicular direction to the basal plane

LIST OF ACRONYMS/ABBREVIATIONS

Al_2O_3	Aluminum Oxide
BVM	Single-phase Brownian Viscosity Model
CFD	Computational Fluid Dynamics
DVM	Single-phase Dispersion Viscosity Model
EEM	Two-phase Eulerian-Eulerian Model
EMM	Two-phase Eulerian-Mixture Model
DA	Directional averaged
FMC	Full Multiphase Coupled
G1	Grid #1
G2	Grid #2
G3	Grid #3
hBN	Hexagonal Boron Nitride
HSPM	Homogeneous Single-phase Model
HSPM-TD	Homogeneous Single-phase Model with Temperature Dependent Properties
PC-SIMPLE	Phase Coupled Semi Implicit Method for Pressure Linked Equations
SIMPLE	Semi Implicit Method for Pressure Linked Equations
SPBM	Single-phase Brownian Model
SPD1	Single-phase Thermal Dispersion Model #1
SPD2	Single-phase Thermal Dispersion Model #2
QUICK	Quadratic Upstream Interpolation for Convective Kinetics
VOF	Volume of Fluid Method

1. INTRODUCTION

1.1. Motivation

Engineered fluids made of a base fluid and nano sized particles such as CuO, Al_2O_3, and TiO_2 [1] that form colloidal suspensions are referred as nanofluids [2]. The most commonly used base fluids are water and ethylene glycol (EG) due to their extensive use in conventional thermal systems. Measured thermal conductivities of nanofluids are found to be exceeding predictions based on the Maxwell's effective medium theory that led many researchers to consider nanofluids as next generation heat transfer fluids [3]. Therefore, nanofluids are considered for many engineering applications such as, cooling of electronics [4, 5], vehicle thermal management [6], and solar energy systems [7, 8].

Application of nanofluids can reduce industrial cost by enhancing thermal conductivity of conventional heat transfer fluids. Studies suggest that addition of nanoparticles by volume fraction of 0.3% in to base fluid, results in significant enhancement of base fluid's thermal conductivity. Furthermore, some nanofluids have interesting futures that can be used in different applications. For example, thermal and rheological characteristics of magnetic nanofluids can be tuned instantaneously by application of an external magnetic field [6]. In the following paragraphs, possible applications of nanofluids to different engineering systems are exemplified.

Ethylene glycol is a commonly used heat transfer fluid in automotive industry as an engine coolant that has poor heat transfer properties compared to that of water. However, its thermal properties can be enhanced by addition of nanoparticles, thus more compact engine cooling systems can be designed [4, 6]. Moreover, manufacturing time, material used, and engine weight can be reduced, leading to more fuel economic and environmentally friendly cars, as a result. Furthermore, since higher heat removal rates can be achieved as a result of enhanced thermal properties, higher horse power engines can be designed. Nanofluids also show a high boiling point that is essential for

maintaining single phase coolant flow at high temperatures. Such characteristic allows design of cooling systems that operate at high temperatures and can remove more heat than existing cooling system [6]. As demonstrated by Tzeng *et al.* [9] nanofluids can also be used in automatic transmission systems where removal of heat generated by rotating parts is important. The study suggests that addition of nanoparticles in to conventional transmission fluid provides cooler operation temperatures.

Thanks to their superior heat transfer characteristics, nanofluids can also be used in cooling of electronics. Today's rapidly developing information technologies (IT) industry, increasing computational demand, and electric powered vehicles require feasible, efficient, and high performance cooling of electronic circuitries, batteries, and other components. Saidur *et al.* [7] pointed out that heat flux generated by processors is expected to rise in the future, thus more effective cooling systems will be needed. Nanofluids can be suggested as a working fluid for heat pipes or in heat spreaders that are widely used in cooling of electronics. Studies suggest that significant improvement in heat transfer rate can be achieved thanks to use of nanofluids in such components. Chein *et al.* [10] reported that by addition of 2% volume fraction of Cu nanoparticles, thermal resistance of a micro-channel heat sink can be reduced by 15%. Jang *et al.* [11], and Chein *et al.* [12] also suggest that addition of nanoparticles enhances cooling performance of micro-channel heat sinks. Application of nanofluids in heat pipes was studied by Tsai *et al.* [13] and Chein *et al.* [14] by considering Au-water and Ag-water nanofluids respectively. Their studies suggest that nanoparticles reduce thermal resistance of heat pipe by 56% and this reduction is a function of particle size. Another application area for the use of nanofluids can be the cooling of batteries of electric powered vehicles by using immersion cooling method. The bottle neck in this approach is that conventional di-electric fluids, such as Ethylene Glycol, have poor thermal properties. However, it is possible to enhance their thermal characteristics by addition of di-electric nanoparticles such as hexagonal boron nitride.

Nanofluids can also be used in medical industry. For example, for drug and radiation delivery, iron based nanoparticles are used as targeting mechanisms of cancer cells. Moreover, nanofluids might be suggested as an effective coolant for cooling

of patient body during critical surgeries to prevent organ damage. Cooling of high power military laser systems can be given as an example for military applications of nanofluids. [6]

One of the interesting property of nanofluids is that their thermal and rheological properties can be adjusted by application of an external magnetic field without changing physical composition of nanofluid. One of the recent topics on nanofluids is the tuning/enhancement of heat transfer characteristic of nanofluids by an external magnetic field. Shima *et al.* [15] reported that thermal conductivity and rheology of magnetic Fe_2O_3-water nanofluids can be tuned by an external magnetic field, and up to 300% enhancement in thermal conductivity can be obtained. Studies of Lajvardi *et al.* [16] and Hong *et al.* [17] reveal that thermal conductivity of magnetic nanoparticles increases under presence of a magnetic field.

1.2. Literature Review

Design and analysis of engineering systems that rely on nanofluids, necessitate accurate estimation of hydrodynamic and thermal characteristics of nanofluids. Many experimental studies have been carried out to quantify thermal characteristics of nanofluids for laminar and turbulent flow conditions [2, 18–31]. However, there are only few studies [32–34] on rheological characterization of nanofluids despite the fact that increase in heat transfer coefficient and Nusselt number is also accompanied by increase in friction factor and pressure drop.

In this section, experimental and numerical studies on laminar flow and forced convection of an Al_2O_3-water nanofluid are discussed. The discussion is divided in to two main headings which are Laminar Forced Convection of Nanofluids and Rheology of Nanofluids.

1.2.1. Laminar Forced Convection of Nanofluids

Forced convection of Al_2O_3-water/EG nanofluids in a uniformly heated tube at fully developed laminar and turbulent flow regimes using a homogeneous single-phase model is studied by Maiga *et al.* [22]. While their predictions underestimate measured heat transfer coefficients, results indicate that addition of nanoparticles enhances convective heat transfer coefficient of Al_2O_3-water nanofluid with 10% particle volume fraction by 60% at a Reynolds number of 250 [22]. Experimental studies such as Zenali *et al.* [18] reported that the increase in convective heat transfer coefficient exceeds that of effective thermal conductivity. This indicates that there are other mechanisms in heat transfer enhancement for forced convection other than the enhancement in thermal conductivity. Single-phase thermal dispersion models are introduced by [21] and [27] to account for energy transport by random movement of nanoparticles, that is also known as thermal dispersion effects. Using thermal dispersion model presented in [21], Özerinç *et al.* [30] studied fully developed laminar forced convection of Al_2O_3-water nanofluid by considering temperature dependent properties. The reported increase in convective heat transfer coefficient of 2.5% Al_2O_3-water nanofluid is 36% at a Peclet number of 6500. The results are in good agreement with the experimental data in the literature, suggesting that single-phase models considering thermal dispersion and temperature dependent properties are capable of predicting heat transfer behavior more accurately.

Mirmasoumi *et al.* [31] investigated mixed convection of Al_2O_3-water nanofluid in a horizontal tube using a two-phase Eulerian-Mixture model. They have shown that particle volume fraction is higher near the wall and bottom of the tube, hence uniform particle distribution is not valid for all cases. Nanofluid forced convection in developing flow in a tube subjected to constant heat flux and temperature was studied by Bianco *et al.* [25] by using single-phase and two-phase Volume of Fluid (VOF), Eulerian-Eulerian (EEM), Eulerian-Mixture (EMM) models considering both constant and temperature dependent properties. According to their results, difference between homogeneous single-phase and two-phase models becomes significant at 11% particle volume fraction. Moreover, it is observed that consideration of temperature dependent properties gives a better estimation of convective heat transfer coefficient.

They observed that convective heat transfer coefficient for 2.5% Al_2O_3-water nanofluid at a Reynolds number of 250 increases up to 17%.

Kalteh *et al.* [28] numerically studied CuO-water nanofluid laminar forced convection in a micro-channel by two-phase EEM. Although velocity and temperature differences between phases are negligible, EEM estimates convective heat transfer coefficient more accurately with respect to single-phase models. They also showed that particle-particle interactions have negligible effect on Nusselt number for laminar flow. Lotfi *et al.* [35] evaluated homogeneous single-phase model, EMM, and EEM for Al_2O_3-water nanofluid. The study neglected temperature dependency of properties and did not include thermal dispersion models. They reported that two-phase models overestimate fully developed heat transfer coefficients, and EMM is the most accurate model among three two-phase models (EEM/EMM/VOF). Akbari *et al.* [26] compared single and two-phase models for mixed convection heat transfer of Al_2O_3-water nanofluid. Their study covers homogeneous single-phase and two phase models (VOF/EMM/EEM) with temperature dependent properties. It is reported that estimated convective heat transfer coefficients by two-phase models are similar. Two-phase models provide more accurate prediction of convective heat transfer coefficient with an overestimation, whereas single-phase model under predicts convective heat transfer coefficient. Although single-phase models are found to be less accurate, it should be noted that the study did not include thermal dispersion models. Single and two-phase models for Al_2O_3-water nanofluid are also studied by Fard *et al.* [23]. They showed that two-phase models provide more accurate prediction of heat transfer of nanofluids for fully developed flow. Despite their computational accuracies, due to increased number of equations to be solved, two-phase models are computationally expensive compared to single-phase models [31,36]. However, there have not been any study that compares prediction accuracies of single and two-phase models while considering their computational costs.

In Section 1.1, it is stated that di-electric nanofluids can be engineered for use in heat transfer applications. Due to being highly thermally conductive [37] and di-electric [38] at the same time, hexagonal boron nitride (hBN) nanoparticles can be used in such

applications. However, due to their graphite like layered atomic structure [39], hBN particles have anisotropic thermal conductivities that are needed to be considered for accurate modeling of nanofluid heat transfer. Although their potential use in nanofluid applications, there are only few studies on characterization of hBN nanofluids. Li *et al.* [40] studied thermal conductivity of hBN and cubic boron nitride nano particles in EG base fluid. The results suggest that, addition of nanoparticles increases thermal conductivity of EG basefluid.

1.2.2. Rheology of Nanofluids

Thermal behavior in forced convection of nanofluids can be accurately modeled by using two-phase models and advanced single-phase models such as thermal dispersion model. However, although they are computationally efficient, single-phase models are not accurate in prediction of nanofluid flow. As shown in [41], while single-phase models predict no change in friction factor, two-phase Eulerian-Eulerian model (EEM) estimates 3% increase for Al_2O_3-water nanofluid flow at a Reynolds number of 1050. Therefore, more advanced and effective viscosity models are needed to increase the accuracy of single-phase models.

Rheological studies [42–49] that have been carried on nanofluids suggest that viscosity of nanofluids μ_{nf} is function of particle size d_p, particle volume fraction φ_p, and nanofluid temperature T. Based on these studies, nanofluids exhibit either non-Newtonian or Newtonian behavior depending on their content [43–46]. Wang *et al.* [44] and Das *et al.* [45] reported that Al_2O_3-water nanofluids for particle volume fractions up to 4% exhibit Newtonian behavior. However, non-Newtonian behavior is observed between shear rates of 0.1 and 1000 1/s for TiO_2-water nanofluid with particle volume fraction of 1.2% [47]. Tseng and Wu [50] studied Al_2O_3-water nanofluid for particle volume fractions between 1 and 16% at different pH values. Non-Newtonian behavior is observed for particle volume fractions of 3-16% for shear rates between 1 and 1000 1/s. In their review, Ding *et al.* [43] concluded that while viscosities of dilute nanofluids are independent of shear rate, nanofluids with high particle volume fractions are more likely to exhibit shear thinning behavior. The review also revealed that nanofluids

with low-viscosity base fluids are more likely to behave non-Newtonian compared to nanofluids with high viscosity base fluids.

Namburu *et al.* [51], Chen *et al.* [46, 52], and Nguyen *et al.* [53] investigated temperature dependency of nanofluid viscosity and reported that nanofluid viscosity strongly depends on temperature as well as particle volume fraction. Chen *et al.* [52] observed that for low shear rates viscosity of nanofluid increases with temperature. However, for high shear rates, viscosity of nanofluid exhibits same characteristics with the base fluid. Nguyen *et al.* showed [53] that beyond a certain temperature, that is referred as critical temperature, properties of nanofluids drastically vary and hysteresis is observed. Such behavior raised questions about reliability of nanofluids in heat transfer applications and indicates that temperature dependency of nanofluid viscosity cannot be neglected.

Since nanofluids tend to agglomerate, they require electrostatical stabilization by adjusting pH value for prolonged stability. Anoop *et al.* [34] investigated effect of electro-viscous effects on effective nanofluid viscosity considering water and EG based nanofluids with Al_2O_3 and CuO particles. The results suggest that viscosity of water based nanofluids is more sensitive to changes in particle volume fraction compared to that of EG based nanofluids, while temperature sensitivity is opposite. It is reported that both nanofluids exhibit Newtonian behavior at shear rates of 10-1000 1/s for particle volume fractions between 0.5 and 6%.

Studies discussed so far revealed that nanofluid viscosity is strongly affected by temperature, and base fluid viscosity. Einstein formula presented in [54] is suggested for dilute ($\varphi_p < 2\%$) nanofluids consisting of spherical particles. Brinkman [55] introduced an extended version of Einstein formulation for moderately concentrated nanofluids up to particle volume fraction of 4%. However, these models consider temperature dependency only through the base fluid viscosity's temperature dependency. To account for temperature effect, Abu-Nada [56] presented a new correlation using experimental data presented in [53]. Masoumi *et al.* [57] and Batchelor [58] proposed viscosity models that include Brownian motion of nanoparticles for nanofluids consisting of rigid spher-

ical particles. Furthermore, Raisee and Moghaddami [33] numerically studied laminar forced convection of Al_2O_3-water nanofluid in a circular pipe. They introduced a Brownian viscosity model based on Brownian thermal conductivity model suggested by Koo and Kleinstreuer [59].

1.3. Objective

Considering the literature, single-phase dispersion models can predict heat transfer coefficient for the cases where data for calibration are available. However, single-phase models fail in prediction of pressure drop. Two-phase models on the other hand, can predict both pressure drop and heat transfer coefficient accurately. However, there is no study that considers the prediction accuracy of recent state-of-the-art nanofluid heat transfer and hydrodynamic models for laminar forced convection of nanofluids. Moreover, present studies do not consider models' computational efficiencies while comparing single and two phase models. Also, none of the studies have focused on numerical methods to increase computational efficiency of Eulerian-Eulerian two-phase model. The literature review also suggests that although their promising physical properties, there are only few studies on characterization of hexagonal boron nitride nanofluids.

Considering the literature, objectives of this study can be listed as follows. The first major objective of this study is to evaluate state-of-the-art single and two phase models in terms of prediction accuracy of convective heat transfer coefficient and pressure drop. Moreover, it is also aimed to provide a comparison of computational efficiencies of single and two phase models, and two different coupling schemes that are used in Eulerian-Eulerian Model. The second major objective of the study is to introduce a dispersion viscosity model to increase single-phase models' pressure drop prediction accuracies. The last objective of the study is to investigate the hBN-water nanofluid's heat transfer performance with two-phase Eulerian-Eulerian and homogeneous single phase models.

1.4. Outline of the Study

In Chapter 2, first mathematical models that are used in modeling of nanofluids are introduced. Then, used numerical methods, domain discretization, and the model validation study are presented in Chapter 3. In Chapter 4 results of the study are presented and discussed.

The results Chapter, is divided into four sections. In Section 4.1 and 4.2, hydrodynamic and thermal results of the study for Al_2O_3-water are presented, respectively. Then in Section 4.3, single and two phase models are compared in terms of their computational efficiencies, and the use of Full Multiphase Coupled scheme for Eulerian-Eulerian model is introduced. In the last section of the chapter, Eulerian-Eulerian and homogeneous single-phase model results for hexagonal boron nitride-water nanofluid are presented.

In Chapter 5, the work that has been carried out is summarized; outcomes of the study are underlined, and suggestions for future works are stated.

2. MATHEMATICAL MODEL

Macroscopic models for nanofluid flow and heat transfer can be classified as single-phase and two-phase models [23,25,26,31]. Single-phase models consider nanoparticles and base fluid as a single homogeneous fluid with respect to its effective properties [22]. On the other hand, two-phase models handle continuity, momentum, and energy equations for particles and base fluid as different continua. This model is suggested for flows where interactions between phases are not well defined [28, 60]. Although two-phase models provide a better understanding of both phases, single-phase models are computationally more efficient, however provide less detail about each phase [28].

For all models presented in this study, effect of body forces and viscous dissipation are neglected as suggested in [22, 23, 26, 28]. For all cases, nanofluid and base fluid are assumed to be incompressible fluids.

2.1. Single-phase Models

Single-phase models assume that base fluid and nanoparticles have the same temperature and velocity field. Therefore, continuity, momentum, and energy equations can be solved as if the fluid were a classical Newtonian fluid by using effective properties of nanofluid. Effective properties are functions of particles size d_p, type, shape, and particle volume fraction φ_p and temperature [2, 21, 22].

Incompressible, steady state continuity equation for single-phase models is given as;

$$\nabla \cdot (\rho_{nf} \vec{v}) = 0 \tag{2.1}$$

where $\vec{v}$ is the velocity vector. Then, steady state momentum and energy equations for

single-phase models [61] can be expressed as;

$$\rho_{nf}\left(\vec{v}\cdot\nabla\vec{v}\right) = -\nabla P + \mu_{eff}\nabla^2\vec{v} \tag{2.2}$$

$$\nabla\cdot\left(\rho_{nf}\vec{v}c_{p,nf}T\right) = \nabla\cdot\left(k_{eff}\nabla T\right) \tag{2.3}$$

where P is the pressure, T is the temperature, $c_{p,nf}$ is the nanofluid specific heat, μ_{eff} is the effective nanofluid viscosity, and k_{eff} is the effective nanofluid thermal conductivity.

2.1.1. Homogeneous Single-phase Model

For the homogeneous single-phase model (HSPM) of Al_2O_3-water nanofluid, constant nanofluid thermal conductivity k_{nf} and viscosity μ_{nf} are considered. These properties are determined by the correlations reported by Hamilton-Crosser [62] and Einstein [54], respectively.

$$\frac{k_{nf}}{k_{bf}} = \frac{k_p + (n-1)k_{bf} - (n-1)(k_{bf}-k_p)\varphi_p}{k_p + (n-1)k_{bf} + (k_{bf}-k_p)\varphi_p} \tag{2.4}$$

$$\frac{\mu_{nf}}{\mu_{bf}} = 1 + 2.5\varphi_p \tag{2.5}$$

where k_{bf} and k_p are the base fluid and nanoparticle thermal conductivities, respectively, and $n = 3$ is the shape factor for spherical particles. However, Hamilton-Crosser equation does not account for temperature dependency of nanofluid thermal conductivity. Thus, correlation reported by Chon *et al.* [63] is also considered and the model is referred as homogeneous single-phase model with temperature dependent properties (HSPM-TD). Since effect of base fluid's temperature dependency on nanofluid thermal conductivity is limited [63], base fluid thermal conductivity is considered as constant. The correlation proposed by Chon *et al.* [63] is given as;

$$\frac{k_{nf}}{k_{bf}} = 1 + 64.7\varphi_p^{0.7460}\left(\frac{d_{bf}}{d_p}\right)^{0.3690}\left(\frac{k_p}{k_{bf}}\right)^{0.7476} Pr^{0.9955}Re_{disp}^{1.2321} \tag{2.6}$$

where d_{bf} is molecular diameter of base fluid (0.29 nm, for water). The Prandtl number Pr and the dispersion Reynolds number Re_{disp} in this correlation are defined as;

$$Pr = \frac{\mu_{bf}}{\rho_{bf}\alpha_{bf}} \tag{2.7}$$

$$Re_{disp} = \frac{\rho_{bf}k_B T}{3\pi\mu_{bf}^2\lambda_{bf}} \tag{2.8}$$

where λ_{bf} is the mean free path between base fluid molecules (0.17 nm, for water), α_{bf} is the thermal diffusivity of base fluid, and $\mu_{bf}(T)$ is the temperature dependent base fluid viscosity (Pa.s) that is defined as follows;

$$\mu_{bf}(T) = 2.414 \times 10^{-5} \times 10^{274.8/(T-140)} \tag{2.9}$$

Effective nanofluid properties for HSPM are defined as;

$$k_{eff} = k_{nf} \tag{2.10}$$

$$\mu_{eff} = \mu_{nf} \tag{2.11}$$

Density ρ_{nf}, and heat capacity of nanofluid $c_{p,nf}$ on the other hand, are estimated by using classical mixture model [23, 25] as follows;

$$c_{p,nf} = \frac{(1-\varphi_p)\, c_{p,bf}\rho_{bf} + \varphi_p c_{p,p}\rho_p}{\rho_{nf}} \tag{2.12}$$

$$\rho_{nf} = (1-\varphi_p)\,\rho_{bf} + \varphi_p\rho_p \tag{2.13}$$

Single-phase models that are presented in following sections are actually improved homogeneous single-phase models in which non-homogeneous nature of nanofluids is represented as additional term in nanofluid's effective properties. For all single-phase models in this study, classical mixture model is used for prediction of nanofluid specific heat and density.

2.1.2. Single-phase Brownian Conductivity Model

Studies have been conducted so far suggest that Brownian motion of nanoparticles is one of the dominant mechanisms that improve nanofluids' energy transport. Therefore, for increased accuracy of single-phase models, this effect should be accounted for. Single-phase Brownian thermal conductivity model (SPBM) is suggested by Koo and Kleinstreuer [59], where Brownian part of effective nanofluid thermal conductivity is defined as a function of particle size, particle volume fraction, and nanofluid temperature as;

$$k_{br} = 5 \times 10^4 \beta(\varphi_p) \varphi_p \rho_{bf} c_{p,bf} \sqrt{\frac{k_B T}{\rho_p D}} f(T, \varphi_p) \tag{2.14}$$

where k_B is the Boltzmann constant, and $\beta(\varphi_p)$ is the fraction of fluid that travels with nanoparticles. Functions $f(T, \varphi_p)$ and $\beta(\varphi_p)$ are presented in [33] as;

$$\begin{aligned} f(T, \varphi_p) =& (-0.8467\varphi_p + 0.0753)T \\ &+ (237.67\varphi_p - 21.998) \end{aligned} \tag{2.15}$$

$$\beta(\varphi_p) = 0.0017(100\varphi_p)^{-0.0841} \tag{2.16}$$

then, the effective nanofluid thermal conductivity can be represented as;

$$k_{eff} = k_{nf} + k_{br} \tag{2.17}$$

Since the model calibration function $f(T, \varphi_p)$ provided in [59] is used, nanofluid thermal conductivity is predicted by Equation 2.4, and the effective nanofluid viscosity for SPBM is defined by Equations 2.11 and 2.5.

2.1.3. Single-phase Brownian Viscosity Model

For single-phase Brownian viscosity model (BVM), it is assumed that energy and momentum transports are enhanced due to Brownian motion of nanoparticles. Here,

the major assumption is that Brownian motion of nanoparticles has an effect like the mixing mechanism, therefore, the expected ratio of momentum and thermal diffusion due to Brownian motion would be similar. Hence, the ratio of momentum diffusion to thermal diffusion, that can be defined in terms of Brownian Prandtl number Pr_{br}, can be considered as unity [33]. Then, Brownian part of the viscosity can be estimated through the nanofluid specific heat.

The effective thermal conductivity of Brownian viscosity model (BVM) is defined by Raisee and Moghaddami [33] through the Hamilton-Crosser and Brownian thermal conductivity models by Equations 2.4 and 2.14, respectively.

The Brownian part of the effective viscosity for BVM can be defined as;

$$\mu_{br} = \frac{k_{br}}{c_{p,nf}} Pr_{br} \tag{2.18}$$

Then, the effective nanofluid viscosity for BVM can be expressed as;

$$\mu_{eff} = \mu_{nf} + \mu_{br} \tag{2.19}$$

Here for BVM, μ_{nf} is determined by Equation 2.5.

2.1.4. Single-phase Thermal Dispersion Model

To account for the effect of Brownian motions of nanoparticles on nanofluid forced convection, Xuan and Roetzel [21] introduced small perturbations in the momentum and energy equations. This effect is then represented as an additional term in nanofluid effective conductivity, and referred as dispersion conductivity k_{disp} that is defined in [21] and [27].

For dispersion models, effective nanofluid conductivity is given as;

$$k_{eff} = k_{nf} + k_{disp} \tag{2.20}$$

The nanofluid thermal conductivity is determined by a correlation such as Equation 2.4. Formulation suggested by Xuan and Roetzel [21] (SPD1) can be given as;

$$k_{disp} = C_1(\rho c_p)_{nf}\varphi_p d_p Ru \tag{2.21}$$

where C_1 is an empirical constant that calibrates model to experimental data, u is the flow velocity in axial direction, and R is the pipe radius. A second formulation that is suggested by Mokmeli and Saffar-Avval [27] (SPD2), can be given as;

$$k_{disp} = C_2(\rho c_p)_{nf}\varphi_p \frac{\partial u}{\partial r}\frac{R}{d_p} \tag{2.22}$$

where C_2 is an empirical constant that calibrates model to experimental data. When C_1 and C_2 are set to zero, both models are reduced to the homogeneous single-phase model.

Nanofluid thermal conductivity for dispersion models here, is predicted by Equation 2.6. The effective nanofluid viscosity for SPD1 and SPD2 is defined by Equation 2.5.

2.1.5. Single-phase Dispersion Viscosity Model

A new single-phase dispersion viscosity model (DVM) is proposed by this study. In the Brownian model suggested by Raisee and Moghaddami [33], it is assumed that effect of nanoparticles' Brownian motion is similar to the mixing mechanism. However, as far as size of the nanoparticles is considered, Brownian motion of particles would not cause any bulk fluid motion. Therefore, it is assumed that Brownian motion of particles is like an additional diffusion mechanism, and Brownian Prandtl number is

assumed to be equal to nanofluid's Prandtl number. The model considers effect of particles' Brownian motion on nanofluid viscosity and thermal conductivity through the thermal dispersion model suggested by Mokmeli and Saffar-Avval [27].

Effective nanofluid thermal conductivity for DVM is defined by using thermal dispersion model that is defined by Equation 2.22. The effective nanofluid viscosity is defined similarly to BVM as;

$$\mu_{eff} = \mu_{nf} + \mu_{disp} \tag{2.23}$$

$$\mu_{disp} = \frac{k_{disp}}{c_{p,nf}} Pr_{br} \tag{2.24}$$

where Pr_{br} is the Brownian Prandtl number, and μ_{nf} is determined by Equation 2.5.

2.2. Two-phase Models

Two-phase models consider continuity, momentum, and energy equations for particles and base fluid as different continua. These models handle continuity, momentum, and energy equations for particles and base fluid using three different methods. First one is the Volume of Fluid (VOF) method, where momentum and energy equations are solved for mixture phase coupled with continuity equation for each phase that describes particle volume fraction [60]. The second method, Eulerian-Mixture model (EMM) is similar to VOF and solves volume fraction equation for particle phase, then relates phase velocities by empirical correlations [35, 60, 64]. The third method is the Eulerian-Eulerian model (EEM) where separate continuity, momentum, and energy equations for each phase are solved [26, 28, 60].

2.2.1. Eulerian-Mixture Model

In Eulerian-Mixture model (EMM), continuity, momentum, and energy equations are solved for the mixture-phase, and the phase velocities are determined by empirical correlations. Steady state, incompressible continuity equation for EMM is given by

Manninen *et al.* [64] as;

$$\nabla \cdot (\rho_m \vec{v}_m) = 0 \tag{2.25}$$

where the mass-averaged velocity or mixture velocity $\vec{v}_m$ for two-phase mixture is defined as;

$$\vec{v}_m = \frac{\rho_p \varphi_p \vec{v}_p + \rho_{bf} \varphi_{bf} \vec{v}_{bf}}{\rho_m} \tag{2.26}$$

where particle and base fluid velocities are represented by $\vec{v}_p$ and $\vec{v}_{bf}$, respectively. φ_p and φ_{bf} are the particle and base fluid volume fractions, and ρ_m is the mixture density for two-phase mixture that is defined as;

$$\rho_m = \varphi_p \rho_p + \varphi_{bf} \rho_{bf} \tag{2.27}$$

The steady state momentum equation for two-phase mixture is;

$$\begin{aligned} \rho_m(\vec{v}_m \cdot \nabla \vec{v}_m) = &- \nabla P + \mu_m \left(\nabla \mu_m + (\nabla \mu_m)^T \right) \\ &+ \nabla \cdot (\varphi_{bf} \rho_{bf} \vec{v}_{dr,bf} \vec{v}_{dr,bf} + \varphi_p \rho_p \vec{v}_{dr,p} \vec{v}_{dr,p}) \end{aligned} \tag{2.28}$$

where P is the pressure, and μ_m is the viscosity of mixture that is equal to base fluid's viscosity ($\mu_m = \mu_{bf}$). $\vec{v}_{dr,p}$ and $\vec{v}_{dr,bf}$ are the drift velocities of particles and base fluid, respectively. Here, $\vec{v}_{dr,p}$ and $\vec{v}_{dr,bf}$ for two-phase mixture are defined as;

$$\vec{v}_{dr,p} = \vec{v}_p - \vec{v}_m \tag{2.29}$$

$$\vec{v}_{dr,bf} = \vec{v}_{bf} - \vec{v}_m \tag{2.30}$$

The slip velocity or relative velocity, represents velocity of the particles $\vec{v}_p$ relative to base fluid $\vec{v}_{bf}$ and it is defined as;

$$\vec{v}_{bf,p} = \vec{v}_{bf} - \vec{v}_p \tag{2.31}$$

The slip and drift velocities are related by following expression:

$$\vec{v}_{dr,p} = \vec{v}_{p,bf} - \left(\frac{\rho_p \varphi_p}{\rho_m} \vec{v}_{bf,p} \right) \tag{2.32}$$

The relative velocity is given by Manninen *et al.* [64] through Schiller and Naumann [65] drag formulation as follows;

$$\vec{v}_{bf,p} = \frac{d_p^2}{18 \mu_{bf} f_d} \frac{\rho_p - \rho_m}{\rho_p} \vec{a} \tag{2.33}$$

$$f_d = \begin{cases} 1 + 0.15 Re_p^{0.687} & \text{if} \quad Re_p \leq 1000 \\ 0.0183 Re_p & \text{if} \quad Re_p > 1000 \end{cases} \tag{2.34}$$

where $\vec{a}$ is the particle's acceleration. The particle Reynolds number Re_p for EMM is defined as;

$$Re_p = \frac{U_m d_p \rho_m}{\mu_m} \tag{2.35}$$

Steady state volume fraction equation for particle phase is defined as;

$$\nabla \cdot (\varphi_p \rho_p \vec{v}_m) = -\nabla \cdot (\varphi_p \rho_p \vec{v}_{dr,p}) \tag{2.36}$$

Steady state energy equation for two-phase mixture is given by Wang and Beckermann [66] as;

$$\nabla \cdot (\varphi_p \vec{v}_p \rho_p i_p + \varphi_{bf} \vec{v}_{bf} \rho_{bf} i_{bf}) = \nabla \cdot (k_{eff} \nabla T) \tag{2.37}$$

where i_{bf} and i_p are the enthalpy of base fluid and particles, respectively. Effective thermal conductivity for two-phase mixture model k_{eff} is defined as;

$$k_{eff} = \varphi_p k_p + \varphi_{bf} k_{bf} \tag{2.38}$$

2.2.2. Eulerian-Eulerian Model

In EEM, momentum and energy equations are solved for each phase. Interactions between phases are defined by additional terms that represent momentum and heat exchange between phases [67]. Since the problem is axis symmetric, 2D steady state, incompressible continuity equation for each phase can be given as;

$$\frac{\partial(\varphi_{bf}\rho_{bf}u_{bf})}{\partial x} + \frac{1}{r}\frac{\partial(r\varphi_{bf}\rho_{bf}v_{bf})}{\partial r} = 0 \tag{2.39}$$

$$\frac{\partial(\varphi_{p}\rho_{p}u_{p})}{\partial x} + \frac{1}{r}\frac{\partial(r\varphi_{p}\rho_{p}v_{p})}{\partial r} = 0 \tag{2.40}$$

where u and v are the velocity components in axial and radial directions, respectively.

For steady flow, axial-momentum equations for base fluid and particles can be given, respectively as;

$$u_{bf}\frac{\partial(\varphi_{bf}\rho_{bf}u_{bf})}{\partial x} + u_{bf}\frac{\partial(\varphi_{bf}\rho_{bf}v_{bf})}{\partial r} = -\varphi_{bf}\frac{\partial P}{\partial x} + \frac{\partial}{\partial x}\left(\varphi_{bf}\mu_{bf}\frac{\partial u_{bf}}{\partial x}\right) + \frac{1}{r}\frac{\partial}{\partial r}\left(\varphi_{bf}\mu_{bf}r\frac{\partial u_{bf}}{\partial r}\right) + (F_d)_x + (F_{vm})_x \tag{2.41}$$

$$u_p\frac{\partial(\varphi_p\rho_p u_p)}{\partial x}+u_p\frac{\partial(\varphi_p\rho_p v_p)}{\partial r}=-\varphi_p\frac{\partial P}{\partial x}+\frac{\partial}{\partial x}\left(\varphi_p\mu_p\frac{\partial u_p}{\partial x}\right)$$
$$+\frac{1}{r}\frac{\partial}{\partial r}\left(\varphi_p\mu_p r\frac{\partial u_p}{\partial r}\right)-(F_d)_x-(F_{vm})_x+(F_{col})_x \tag{2.42}$$

Similarly, the radial-momentum equations can be written as;

$$v_{bf}\frac{\partial(\varphi_{bf}\rho_{bf}u_{bf})}{\partial x}+v_{bf}\frac{\partial(\varphi_{bf}\rho_{bf}v_{bf})}{\partial r}=-\varphi_{bf}\frac{\partial P}{\partial r}+\frac{\partial}{\partial x}\left(\varphi_{bf}\mu_{bf}\frac{\partial v_{bf}}{\partial x}\right)$$
$$+\frac{1}{r}\frac{\partial}{\partial r}\left(\varphi_{bf}\mu_{bf}r\frac{\partial v_{bf}}{\partial r}\right)-\mu_p\frac{v_{bf}}{r^2}+(F_d)_r+(F_{vm})_r \tag{2.43}$$

$$v_p\frac{\partial(\varphi_p\rho_p u_p)}{\partial x}+v_p\frac{\partial(\varphi_p\rho_p v_p)}{\partial r}=-\varphi_p\frac{\partial P}{\partial r}+\frac{\partial}{\partial x}\left(\varphi_p\mu_p\frac{\partial v_p}{\partial x}\right)$$
$$+\frac{1}{r}\frac{\partial}{\partial r}\left(\varphi_p\mu_p r\frac{\partial v_p}{\partial r}\right)-\mu_p\frac{v_p}{r^2}-(F_d)_r-(F_{vm})_r+(F_{col})_r \tag{2.44}$$

where $\vec{F}_{vm}$ is the virtual mass force due to relative acceleration of phases [60]. Since it has negligible effect on heat transfer as shown by Kalteh *et al.* [28], it is neglected in this study. $\vec{F}_{col}$ is particle-particle collision force, and $\vec{F}_d$ is the drag force between the fluid and solid phases defined by phase interaction equations. The drag force between phases is defined as;

$$\vec{F}_d=-\zeta(\vec{v}_{bf}-\vec{v}_p) \tag{2.45}$$

where ζ is the friction factor which depends on particle size and particle volume fraction. For dilute solutions, ($\varphi_{bf}>0.8$) ζ is defined by Syamlal and Gidaspow [67] as;

$$\zeta=\frac{3}{4}C_d\frac{\varphi_{bf}\varphi_p}{d_p}|\vec{v}_{bf}-\vec{v}_p|\varphi_{bf}^{-2.65} \tag{2.46}$$

where C_d is the drag coefficient and can be predicted as;

$$C_d=\begin{cases}\dfrac{24}{Re_p}(1+0.15Re_p^{0.697}) & \text{if} \quad Re_p<1000\\ 0.44 & \text{if} \quad Re_p\geq 1000\end{cases} \tag{2.47}$$

where particle Reynolds number Re_p is defined as;

$$Re_p = \frac{\varphi_{bf}\rho_{bf}|\vec{v}_{bf} - \vec{v}_p|d_p}{\mu_{bf}} \tag{2.48}$$

Collision force of particles $\vec{F}_{col}$ is defined by Bouillard *et al.* [68] as;

$$\vec{F}_{col} = G(\varphi_{bf})\nabla\varphi_{bf} \tag{2.49}$$

where $G(\varphi_{bf})$ is the particle-particle interaction modulus and it is defined as;

$$G(\varphi_{bf}) = exp\left[-600(\varphi_{bf} - 0.376)\right] \tag{2.50}$$

Once momentum equations for each phase and the related phase interaction equations are defined, steady state energy equation for each phase can be presented as follows;

$$\begin{gathered}\frac{\partial}{\partial x}(\varphi_{bf}\rho_{bf}u_{bf}c_{p,bf}T_{bf}) + \frac{\partial}{\partial r}(\varphi_{bf}\rho_{bf}v_{bf}c_{p,bf}T_{bf}) = \\ \frac{\partial}{\partial x}\left(\varphi_{bf}k_{eff,bf}\frac{\partial T_{bf}}{\partial x}\right) + \frac{1}{r}\frac{\partial}{\partial r}\left(\varphi_{bf}k_{eff,bf}r\frac{\partial T_{bf}}{\partial r}\right) - h_v(T_{bf} - T_p)\end{gathered} \tag{2.51}$$

$$\begin{gathered}\frac{\partial}{\partial x}(\varphi_p\rho_p u_p c_{p,p}T_p) + \frac{\partial}{\partial r}(\varphi_p\rho_p v_p c_{p,p}T_p) = \\ \frac{\partial}{\partial x}\left(\varphi_p k_{eff,p}\frac{\partial T_p}{\partial x}\right) + \frac{1}{r}\frac{\partial}{\partial r}\left(\varphi_p k_{eff,p}r\frac{\partial T_p}{\partial r}\right) + h_v(T_{bf} - T_p)\end{gathered} \tag{2.52}$$

where $k_{eff,p}$ and $k_{eff,bf}$ are the effective thermal conductivity of base fluid and particles, and h_v is volumetric interphase heat transfer coefficient between phases. The temperature for particle and base fluid phases are T_p, and T_{bf}, respectively. Volumetric

interphase heat transfer coefficient is defined as;

$$h_v = \frac{6(1-\varphi_{bf})}{d_p} h_p \tag{2.53}$$

For mono dispersed particles, particle heat transfer coefficient h_p is estimated by Wakao and Kagei [69] through the particle Nusselt number Nu_p as follows;

$$Nu_p = \frac{h_p d_p}{k_{bf}} = 2 + 1.1 Re_p^{0.6} Pr^{1/3} \tag{2.54}$$

where Pr is the liquid phase Prandtl number. The particle Reynolds number is defined by Equation 2.48. The effective conductivities for particle and base fluid phases can be given as [70];

$$k_{eff,bf} = \frac{k_{b,bf}}{\varphi_{bf}} \tag{2.55}$$

and

$$k_{eff,p} = \frac{k_{b,p}}{\varphi_p} \tag{2.56}$$

where $k_{b,bf}$ and $k_{b,p}$ are defined as;

$$k_{b,bf} = (1 - \sqrt{1-\varphi_{bf}}) k_{bf} \tag{2.57}$$

$$k_{b,p} = (\sqrt{1-\varphi_{bf}})(\omega A + [1-\omega]\Gamma) k_{bf} \tag{2.58}$$

with $\omega = 7.26 \times 10^{-3}$ for spherical particles and Γ is defined as;

$$\Gamma = \frac{2}{1-\frac{B}{A}} \left(\frac{B(A-1)}{A\left(1-\frac{B}{A}\right)^2} ln\left(\frac{A}{B}\right) - \frac{B-1}{1-\frac{B}{A}} - \frac{B+1}{2} \right) \tag{2.59}$$

where parameters A, and B for a spherical particle are given as;

$$A = \frac{k_p}{k_{bf}} \tag{2.60}$$

$$B = 1.25\left(\frac{1-\varphi_{bf}}{\varphi_{bf}}\right)^{10/9} \tag{2.61}$$

3. PROBLEM STATEMENT AND NUMERICAL METHOD

In this chapter, problem domain and numerical methods that are used in the study are presented. Furthermore, domain discretization, used numerical methods, and applied boundary conditions for single and two phase models are explained. In last section, results of model validation and grid independency studies are discussed.

3.1. Problem Domain

The problem domain is selected by considering availability of experimental data in literature. The experimental setup presented by Wen and Ding [24] is considered, and dimensions of domain that is shown in Figure 3.1, are selected accordingly. Since the problem is axisymmetric, the 3D problem domain that is shown in Figure 3.1 is reduced to a 2D domain in order to increase computational efficiency. A uniform structured grid with quadrilateral elements is used for domain discretization. Detailed information regarding the grid and the grid independency study is presented in Section 3.4. Since the all elements are same for the entire domain, only the actual grid at the beginning of the domain is shown in Figure 3.2.

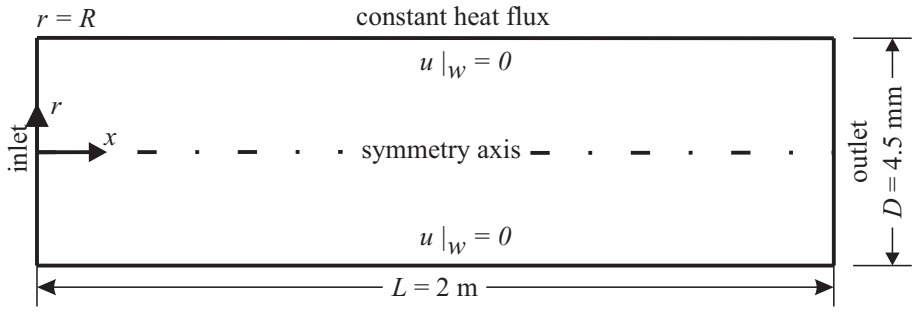

Figure 3.1. Problem domain.

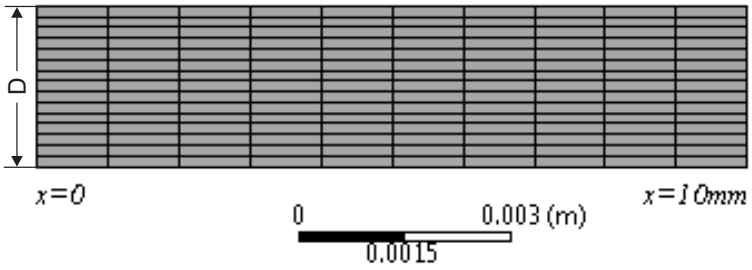

Figure 3.2. Section of the grid that is used in discretization of the domain.

3.2. Numerical Methods

Finite Control Volume method is used to solve numerically the equations for nanofluid flow and heat transfer. For single-phase model, momentum, energy, and continuity equations are solved with effective nanofluid properties. For both single and two phase models, third order power-law scheme are used discretization of momentum, energy, and pressure equations, respectively. Semi Implicit Method for Pressure Linked Equations (SIMPLE) algorithm is used for and velocity pressure coupling in single-phase and two-phase Eulerian-Mixture models. For, EEM and EMM, the third order Quadratic Upstream Interpolation for Convective Kinetics (QUICK) scheme is used to solve volume fraction equation.

The Phase Coupled SIMPLE (PC-SIMPLE) algorithm is used for pressure and velocity coupling in EEM and EMM. However, for EEM, in addition to PC-SIMPLE algorithm that is widely used in literature, a different algorithm, namely Full Multi-phase Coupled (FMC), is used for coupling scheme to assess its accuracy and efficiency. PC-SIMPLE is a well-established, widely used, and robust algorithm, where phase velocities are solved in a segregated manner with a pressure correction. Whereas in FMC algorithm, velocity, shared pressure, and volume fraction corrections are coupled simultaneously. Although FMC algorithm is expected to be more efficient, divergence may occur at high particle volume fractions due to volume fraction equation [60]. A convergence criterion is used so that residuals for all equations are less than 1×10^{-6}.

3.3. Boundary Conditions

3.3.1. Single-phase Models

Boundary conditions for governing equations of single-phase model are defined considering the no-slip condition at the wall;

$$u(x, R) = v(x, R) = 0 \tag{3.1}$$

and uniform inlet velocity at the inlet

$$u(0, r) = U \quad v(0, R) = 0 \tag{3.2}$$

with constant wall heat flux q''_{wall} condition that is expressed as;

$$-k_{eff} \frac{\partial T}{\partial r}\bigg|_{wall} = q''_{wall} \tag{3.3}$$

Dispersion model empirical constants C_1 and C_2 in Equations 2.21 and 2.22 are determined accordingly to the experimental data presented by Wen and Ding [24].

3.3.2. Eulerian-Mixture Model

Boundary conditions for EMM are defined based on no-slip condition at wall for mixture phase as;

$$u_m(x, R) = v_m(x, R) = 0 \tag{3.4}$$

and uniform inlet velocity for base fluid and particle phases, respectively.

$$u_{bf}(0,r) = U_{bf} \quad v_{bf}(0,r) = 0 \tag{3.5}$$

$$u_{p}(0,r) = U_{p} \quad v_{p}(0,r) = 0 \tag{3.6}$$

where $U_p = U_{bf}$ are mean velocities of base fluid and particles. Uniform constant heat flux at wall is applied as;

$$-k_{eff}\frac{\partial T}{\partial r}\bigg|_{wall} = q''_{wall} \tag{3.7}$$

3.3.3. Eulerian-Eulerian Model

Similarly to EMM, the boundary conditions for EEM are defined with respect to no-slip condition at wall boundaries for base fluid and particles phase as;

$$u_{bf}(x,R) = v_{bf}(x,R) = 0 \tag{3.8}$$

$$u_{p}(x,R) = v_{p}(x,R) = 0 \tag{3.9}$$

with uniform inlet velocity for base fluid and particle phases as;

$$u_{bf}(0,r) = U_{bf} \quad v_{bf}(0,r) = 0 \tag{3.10}$$

$$u_{p}(0,r) = U_{p} \quad v_{p}(0,r) = 0 \tag{3.11}$$

and constant wall heat flux for particle fluid mixture as;

$$-\left(\varphi_p k_{eff,p}\frac{\partial T_p}{\partial r}\bigg|_{wall} + \varphi_{bf} k_{eff,bf}\frac{\partial T_{bf}}{\partial r}\bigg|_{wall}\right) = q''_{wall} \tag{3.12}$$

3.4. Model Validation

A grid independence study is carried out in order to ensure grid independent solutions. Three different grid resolutions are compared with correlation given by Shah and London [71] and experimental data reported by Wen and Ding [24]. The validation of the models and the grid independency of the solutions are presented in Figure 3.3. The Shah correlation used in this study can be given as;

$$\frac{Nu_x + 1}{L} = \left[1 + \left(\frac{\pi/(115.2x^*)}{M^{0.5}N^{3/5}}\right)^{5/3}\right]^{3/10} \tag{3.13}$$

$$L = 5.364\left\{1 + [(220/\pi)x^*]^{-10/9}\right\}^{3/10}$$

$$M = 1 + (Pr/0.0207)^{2/3}$$

$$N = 1 + [(220/\pi)x^*]^{-10/9}$$

where the local Nusselt number Nu_x and dimensionless axial distance x^* are defined as;

$$Nu_x = \frac{h(x)D}{k_{bf}} = \frac{q''_{wall}D}{k_{bf}(T_{wall} - T_{mean})} \tag{3.14}$$

$$x^* = \frac{x}{DRePr} \tag{3.15}$$

$$Re = \frac{\rho_{bf}DU}{\mu_{bf}} \tag{3.16}$$

For nanofluids, Reynolds number is defined as;

$$Re_{nf} = \frac{\rho_{nf}DU_{nf}}{\mu_{nf}} \tag{3.17}$$

and for both two-phase and single-phase models, Nu_x for nanofluid is defined as;

$$Nu_{nf,x} = \frac{h(x)D}{k_{nf}} = \frac{q''_{wall}D}{k_{nf}(T_{wall} - T_{mean})} \tag{3.18}$$

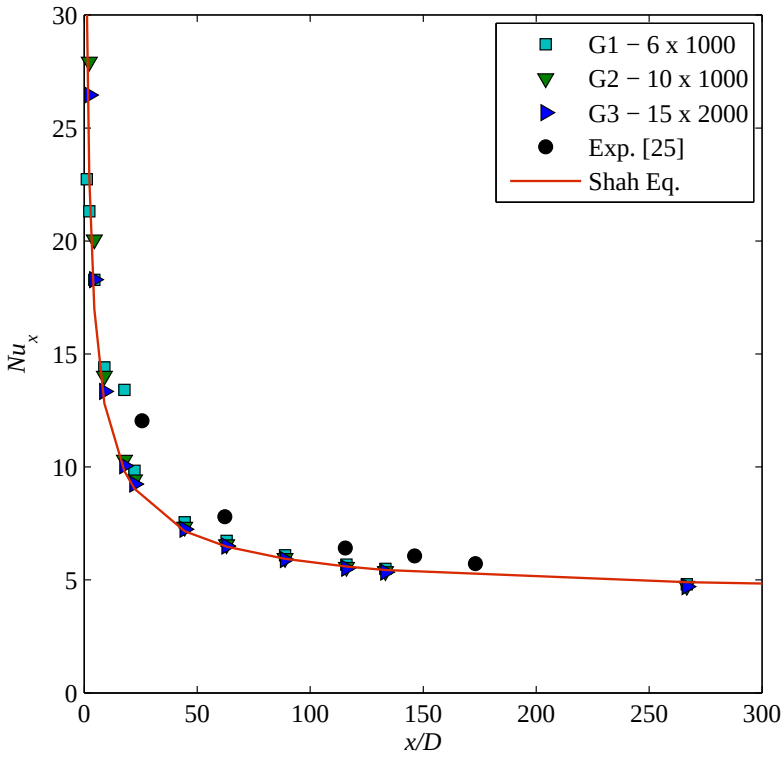

Figure 3.3. Comparison of different grid solutions with experiment and Equation 3.13 for laminar forced convection of pure water at entry region for Re=1050.

Grid independency analysis reveals that grid #2 (G2) and grid #3 (G3) show less than 1% deviation from each other. Hence, solutions of G2 and G3 can be considered as grid independent. Figure 3.3 indicates that for pure water, results of G2 and G3 agree well with Equation 3.13. On the other hand, single-phase model shows maximum 15% deviation from experimental results [24]. Variation of local Darcy friction factor f_x was also checked and presented in Figure 3.4 for different grids. Results indicate that G3 has 0.7% error with respect to theoretical value of Darcy friction factor for the fully developed region. Darcy friction factor used here is defined as;

$$f_x = \frac{8\tau_w(x)}{\rho_{bf}U^2} \tag{3.19}$$

where $\tau_w(x)$ is local wall shear stress, U is the mean axial velocity.

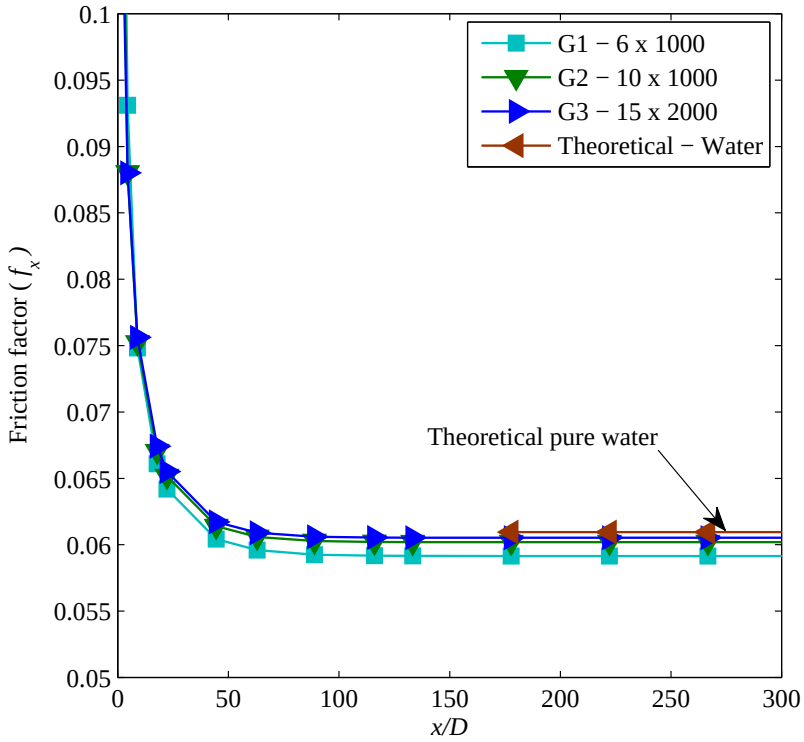

Figure 3.4. Comparison of friction factor of different grid resolutions (G1, G2, G3) for pure water.

4. RESULTS

In this chapter, numerical results of convective heat transfer of nanofluid flow in a circular duct are presented. The numerical analysis is performed using single and two phase models that include homogeneous single-phase, single-phase dispersion, single-phase Brownian, two-phase Eulerian-Eulerian, and two-phase Eulerian-Mixture models. Details about each model such as, geometry definition, boundary conditions, and numerical methods are presented in Chapters 2 and 3 in detail. Single-phase models and their effective viscosity and thermal conductivity models are listed in Table 4.1 to clarify any ambiguity regarding definition of single-phase models.

The results in this section are presented under four sections. These are, Hydrodynamic Results, Thermal Results, Computational Efficiency of Models, and Hexagonal Boron Nitride Study. In the first three sections, hydrodynamic and thermal prediction accuracies, and numerical efficiencies of models are discussed for Al_2O_3-water nanofluid. Then, in the last section, results of single-homogeneous and two-phase Eulerian-Eulerian models for hexagonal boron nitride-water nanofluid are presented. Part of the results that are presented here are published in [41,72,73]. Unless otherwise

Table 4.1. Single-phase models and corresponding effective property models.

Model Name	**Thermal Conductivity Model(s)**		**Viscosity Model(s)**	
	k_{nf}	k_{disp} or k_{br}	μ_{nf}	μ_{disp} or μ_{br}
HSPM	Equation 2.4	0	Equation 2.5	0
HSPM-TD	Equation 2.6	0	Equation 2.5	0
SPD1	Equation 2.6	Equation 2.21	Equation 2.5	0
SPD2	Equation 2.6	Equation 2.22	Equation 2.5	0
SPBM	Equation 2.4	Equation 2.14	Equation 2.5	0
DVM	Equation 2.6	Equation 2.22	Equation 2.5	Equation 2.24
BVM	Equation 2.4	Equation 2.14	Equation 2.5	Equation 2.18

is stated, all results presented in this study belong to author.

4.1. Hydrodynamic Results

In this section, solutions of homogeneous single-phase model (HSPM), single-phase Brownian viscosity model (BVM), single-phase dispersion viscosity model (DVM) that is proposed by this study, two-phase Eulerian-Eulerian model (EEM), and two-phase Eulerian-Mixture model (EMM) are compared with experimental data presented by Hwang *et al.* [32] for a Reynolds number range of 400-620.

Velocity profiles of HSPM, BVM, DVM, EMM, and EEM for 0.3% Al_2O_3-water nanofluid at Reynolds number of 501 are compared with theoretical velocity profile of water and it is observed that all models predict similar velocity profiles.

Results suggest that for 0.3% Al_2O_3-water nanofluid, EEM is the most accurate model in predicting pressure drop among models considered in this study. For the Reynolds number range considered, the error between experimental data and EEM are between 3.0% and 9.3%, respectively.

For the BVM model that has been proposed by Raisee and Moghaddami [33], it is assumed that Brownian motion of nanoparticles inside a base fluid mimics the mixing mechanism in turbulence, thus Brownian Prandtl number is assumed to be unity. However, Brownian motion does not induce a bulk movement in the fluid. Therefore, it is more suitable to interpret the Brownian motion or dispersion effects as an additional diffusion mechanism than a mixing mechanism. This is demonstrated by comparison of DVM with Brownian Prandtl number is equal to unity and nanofluid's Prandtl number (6.97). Comparison of DVM for $Pr_{br} = 1$ and $Pr_{br} = 6.97$ with other models can be found in Figures 4.1 and 4.2. A similar comparison for BVM is also done, but since results indicated a negligible difference between $Pr_{br} = 1$ and $Pr_{br} = 6.97$, results corresponding to BVM for $Pr_{br} = 6.97$ are not plotted. It is observed that taking Brownian Prandtl number equal to nanofluid's Prandtl number has negligible effect on convective heat transfer prediction accuracy of the model. Overall, the results

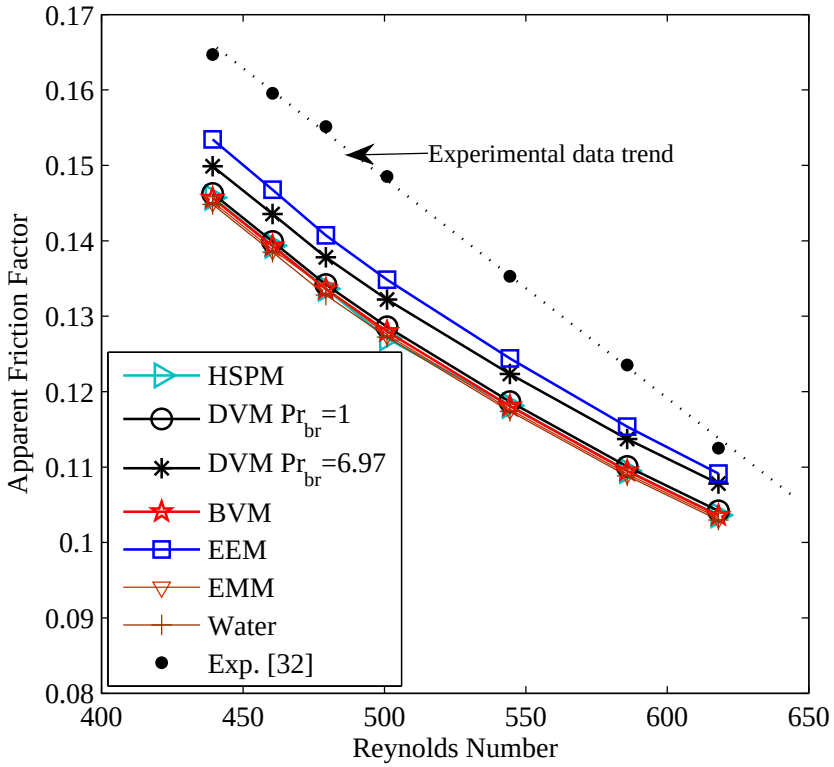

Figure 4.1. Comparison of apparent friction factors of models for 0.3% Al_2O_3-water.

suggest that interpretation of Brownian motion or dispersion effects as an additional diffusion mechanism is a reasonable assumption.

The apparent friction factors f_{app} predicted by models are compared in Figure 4.1. Similarly to the pressure drop results, predicted apparent friction factor by the EEM is the most accurate with respect to experimental data. Error values for EEM with respect to experimental data [32] are between 3.0-9.3%. As expected, the apparent friction factor is underestimated by other models. The error values for these models are 7.9-13.9%, 4.2-11.2%, 7.9-14.4%, and 8.2-14.1% for BVM, DVM with Pr_{br}=6.97, HSPM, and EMM, respectively. It is also observed that all of the models considered here follow the experimental trend with a slight deviation. The figure suggests that models tend to be more accurate as the Reynolds number increases. Results also suggest that DVM model accuracy increased by 2%, as a result of dispersion mechanism assumption. Therefore, DVM is the most accurate single-phase model in prediction of pressure drop and friction factor.

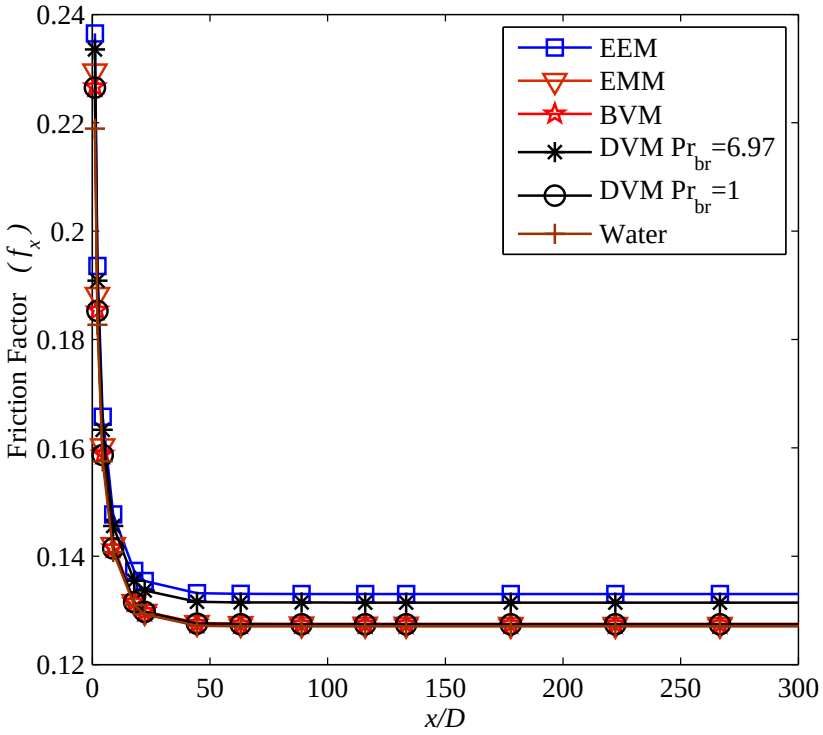

Figure 4.2. Comparison of friction factors of models for 0.3% Al_2O_3-water at $Re_{nf} = 501$.

The apparent friction factor f_{app} is defined as;

$$f_{app} = \frac{\Delta P}{\frac{1}{2}\rho_{nf} U_{nf}^2} \cdot \frac{D}{L} \tag{4.1}$$

In Figure 4.2 comparison of predicted friction factor versus axial distance is presented for a Reynolds number of 501 for 0.3% Al_2O_3-water. Since there are no experimental data for friction factor change in developing flow, single-phase models and EMM are compared with EEM model. Although DVM can be further calibrated to exactly match the experimental data, such calibration would have an effect on thermal solution of DVM, since the model is calibrated accordingly to the experimentally obtained heat transfer coefficient. The increase observed in friction coefficient is due to the Brownian part of the nanofluid viscosity.

4.2. Thermal Results

In this section, numerical results of homogeneous single-phase model (HSPM), single-phase thermal dispersion models, single-phase Brownian model (SPBM), two-phase Eulerian-Eulerian model (EEM), and two-phase Eulerian-Mixture model (EMM) for forced convection of Al_2O_3-water nanofluid are discussed and compared with experimental and numerical data presented by Wen and Ding [24] and Akbari *et al.* [26], respectively.

In Figure 4.3, Nusselt number predictions of each model are compared with experimental [24] and numerical [26] results from the literature. Results suggest that single-phase models underestimate Nu_x at the entry region, whereas both two-phase models overestimate Nu_x, as can be seen from Figure 4.3. Error with respect to experimental values are -34.87% and -76.16% at $x/D = 63$ and $x/D = 116$, respectively for HSPM. For EEM, error values are -0.9% and -7.7% at the same locations, respectively. Nu_x predictions of EMM and EMM reported by Akbari *et al.* [26] are very close to

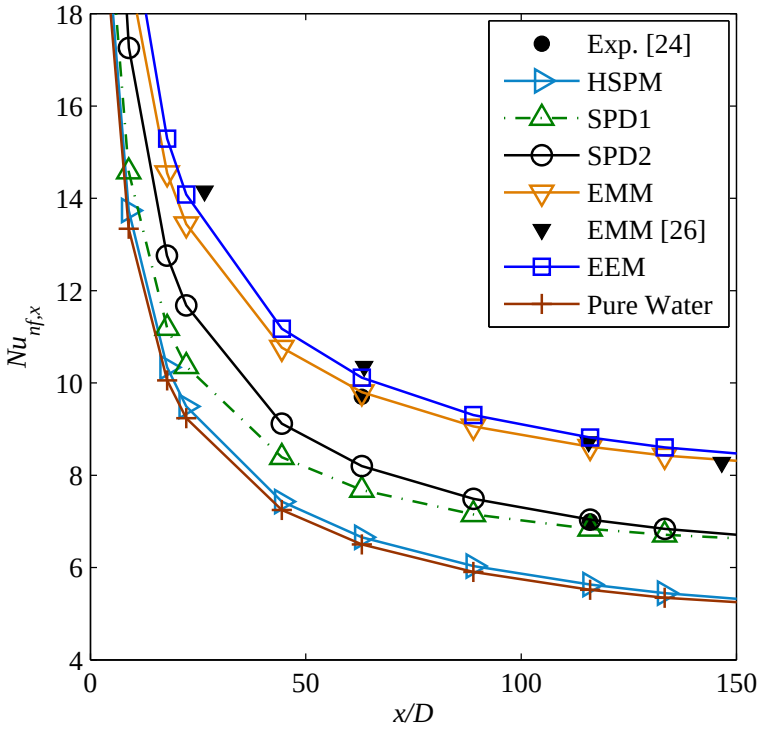

Figure 4.3. Comparison of predicted Nusselt numbers of single-phase and two-phase models for 1.6% Al_2O_3-water at $Re_{nf} = 1050$.

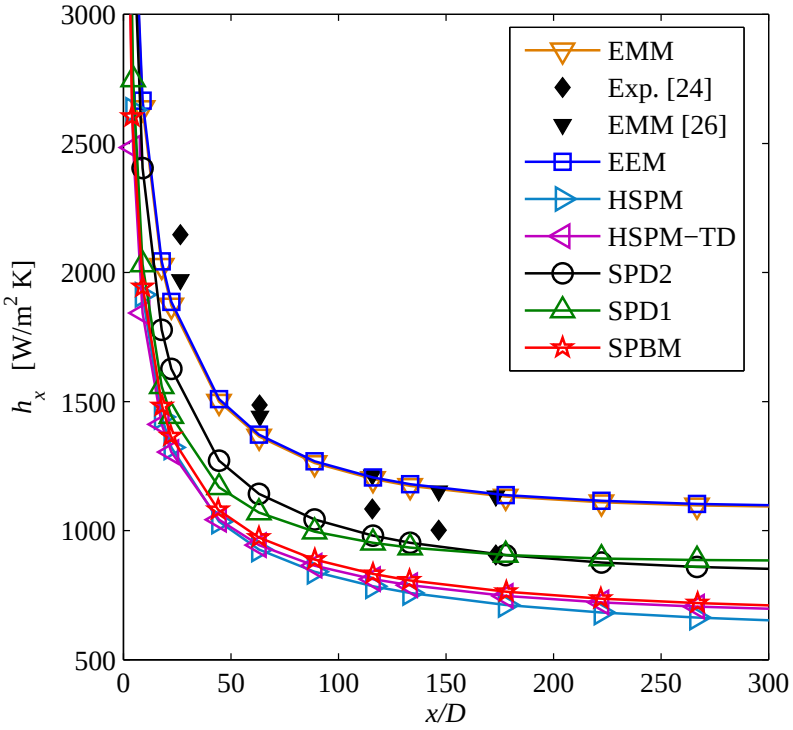

Figure 4.4. Comparison of predicted convective heat transfer coefficients by single and two phase models with experimental data at Re_{nf}=1050 for 1.6% Al_2O_3-water nanofluid.

each other. The slight difference between models might be due to variation of thermophysical properties of Al_2O_3 used. In this study thermophysical properties of Al_2O_3 are taken from National Institute for Standards and Technology [74]. An additional comparison with experimental data presented by Wen and Ding [24] in terms of local convective heat transfer coefficient h_x versus x/D is also presented in Figures 4.4-4.5 to prevent any possible ambiguity due to definition of nanofluid thermal conductivity.

Figure 4.4 indicates that at the beginning of entry region, effect of temperature dependency of properties on the solution is limited, since the flow is not fully affected by the thermal boundary conditions. As it can be seen from comparison of HSPM and HSPM-TD, the effect increases as the flow develops. Table 4.2 suggests that use of temperature dependent nanofluid conductivity model results in 4% increase in solution accuracy of single-phase models for particle volume fraction of 1.6%. The other temperature dependent thermal conductivity model that is considered is SPBM. The model is found to be 2% more accurate in prediction of convective heat transfer

Table 4.2. Error in predicted convective heat transfer coefficient of 1.6% Al_2O_3-water for $Re_{nf} = 1050$.

	$x/D = 22$	$x/D = 63$	$x/D = 116$	$x/D = 178$
EEM	−12.1%	−7.7%	11.3%	25.6%
EMM	−12.8%	−8.1%	10.8%	25.0%
HSPM	−38.4%	−37.6%	−27.3%	21.3%
SPD1	−32.8%	28.0%	−12.1%	0.0%
SPD2	−24.2%	−23.1%	−9.5%	0.1%
SPBM	−36.4%	−34.5%	−23.2%	−15.7%

coefficient compared to that of HSPM-TD. The comparison of dispersion models reveals that SPD2, that uses dispersion conductivity formulation by Equation 2.22, is more accurate in predicting heat transfer coefficient at entry region compared to SPD1, which uses formulation by Equation 2.21. As shown in Table 4.2, SPD2 model is approximately 8% more accurate in predicting heat transfer coefficient at the entry region compared to SPD1. In Table 4.2 and Figure 4.4, it is also shown that for particle volume fraction of 1.6% at a Reynolds number of 1050, predictive accuracy of EMM becomes superior to that of EEM as the flow develops. It is also observed that both EEM and EMM start over-predicting convective heat transfer coefficient as flow develops. Overall, EMM and EEM are found to be 12% more accurate than SPD2 at the entry region for particle volume fraction of 1.6%.

Based on Figures 4.5 and 4.6, and Tables 4.2-4.4, it can be concluded that the best single-phase model is SPD2. However, there is no clear indication on the best two-phase model, since both EEM and EMM have similar accuracies at different particle volume fractions as shown in Tables 4.2-4.4. The difference in error values of EEM and EMM can be neglected as far as experimental uncertainties are considered. The results indicate that EEM is the most accurate model up to axial distance of $x/D = 116$. After that point EMM model becomes the most accurate model. Tables 4.2-4.4 do not indicate a distinct relation between model accuracies and particle volume fraction for two-phase models at the entry region. However at the fully developed region, as particle

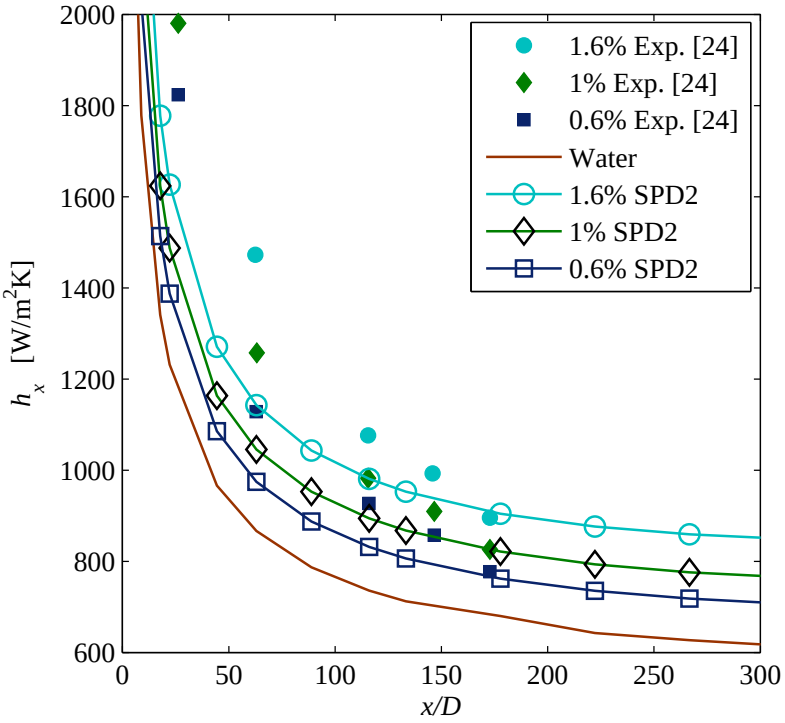

Figure 4.5. Comparison of predicted convective heat transfer coefficients by SPD2 at $Re_{nf} = 1050$ for 0.6%, 1%, and 1.6% Al_2O_3-water nanofluid.

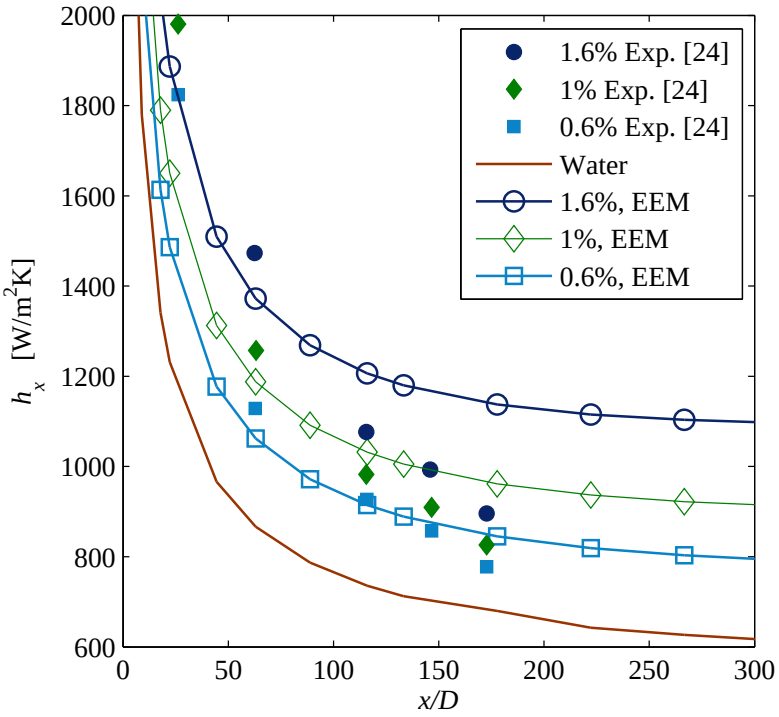

Figure 4.6. Comparison of predicted convective heat transfer coefficients by EEM at $Re_{nf} = 1050$ for 0.6%, 1%, and 1.6% Al_2O_3-water nanofluid.

Table 4.3. Error in predicted convective heat transfer coefficient of 1% Al_2O_3-water for $Re_{nf} = 1050$.

	$x/D = 22$	$x/D = 63$	$x/D = 116$	$x/D = 178$
EEM	−16.7%	−5.7%	4.4%	15.5%
EMM	−17.4%	−6.2%	3.9%	14.9%
HSPM	−36.6%	−29.5%	−23.6%	−17.3%
SPD1	−31.0%	21.0%	−11.7%	−1.7%
SPD2	−24.9%	−17.0%	−9.5%	−1.3%
SPBM	−33.2%	−25.6%	−18.7%	−11.7%

volume fraction decreases the error of both single and two phase models decrease.

The prediction accuracies of SPD2 and EEM are investigated at different particle volume fractions in Figures 4.5 and 4.6 with Tables 4.2-4.4. Results indicate that, EEM model underestimates convective heat transfer coefficient at the beginning of entry region, where SPD2 under predicts until the calibration point ($x/D = 176$). However as flow develops, EEM starts overestimating the convective heat transfer coefficient. Results in Tables 4.2-4.4 also suggest that calibration constant for SPD2 is independent of particle volume fraction, as far as uncertainties in experimental results are concerned. It is also observed that the error of SPD2 and EEM at a given axial

Table 4.4. Error in predicted convective heat transfer coefficient of 0.6% Al_2O_3-water for $Re_{nf} = 1050$.

	$x/D = 22$	$x/D = 63$	$x/D = 116$	$x/D = 178$
EEM	−14.4%	−6.0%	−0.6%	8.5%
EMM	−19.2%	−6.5%	−1.2%	7.8%
HSPM	−31.4%	−22.0%	−18.8%	−12.6%
SPD1	−27.8%	−16.2%	−10.9%	2.0%
SPD2	−23.8%	−13.6%	−9.6%	1.6%
SPBM	−29.0%	−18.6%	−14.9%	−8.2%

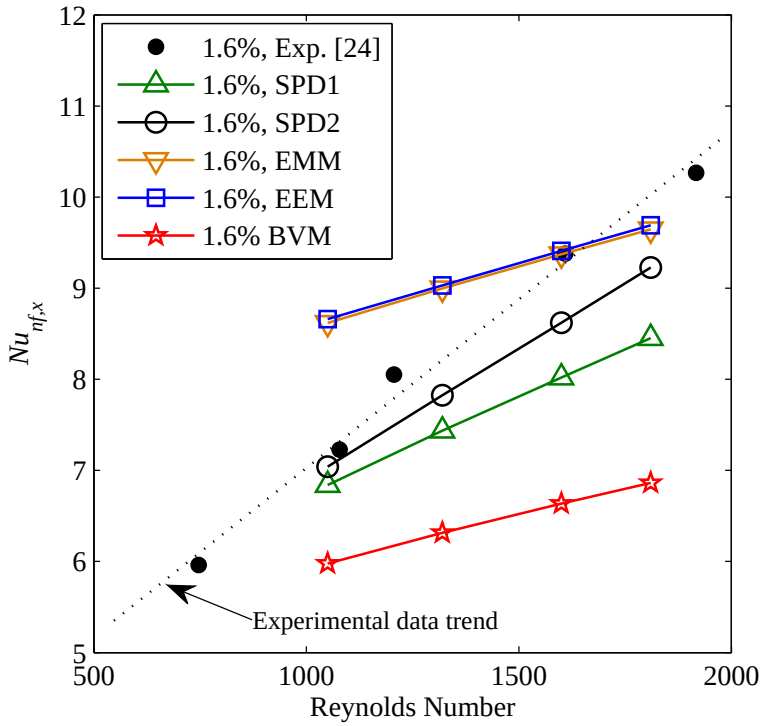

Figure 4.7. Comparison of models in predicting Nu_x of 1.6% Al_2O_3-water nanofluid at $x/D = 116$ for Reynolds numbers of 1050, 1320, 1600, 1810.

distance are at the same order of magnitude for all three particle volume fractions. It is seen that the both models perform best near the calibration point as expected. Hence if required, SPD2 model can be calibrated such that the model would be accurate at a specified point.

Accuracy of models at different Reynolds numbers is also investigated in terms of Nusselt number for particle volume fraction of 1.6%. In Figure 4.7, Nusselt number predictions of models at different Reynolds numbers (1050, 1320, 1600, 1810) are shown and the results are compared with experimental data [24]. Both dispersion models are calibrated based on the experimental data [24] at axial location of $x/D = 178$ for Reynolds number of 1050 and particle volume fraction of 1.6%.

Comparison of models in Figure 4.7 reveals that SPD2 is the most accurate model in predicting Nusselt number for the Reynolds numbers range considered. Despite considering each phase individually, EMM and EMM underestimate the change in Nusselt number with changing Reynolds numbers. Although SPD2 is calibrated for Reynolds

number of 1050, the model can predict the experimental trend data accurately. Since desired accuracy can be achieved with a single calibration for different particle volume fractions and Reynolds numbers, SPD2, is suggested for applications where calibration data is available. On the other hand, for nanofluids with no prior experimental studies, one of the two-phase models is suggested.

4.3. Computational Efficiency of Models

Macroscopic models play a key role in both integration of nanofluids to existing engineering systems, and design of devices or systems that rely on nanofluids. Therefore, macroscopic models should be both robust and efficient. In this section, computational efficiencies of single and two phase models are compared, and application of a more efficient algorithm, that is Full Multiphase Coupled, is demonstrated. The numerical studies that are presented in this study have been performed on a workstation operating with a Quad Core 2.4GHz CPU, and all four cores were used in calculations.

The major drawback of two-phase models is their computational expense due to increased number of equations to be solved. As shown in Table 4.8, the required CPU time is 163.79 seconds for EEM when PC-SIMPLE algorithm is used, 81.68 seconds for single-phase models, and 566.50 seconds for EMM for 1.6% Al_2O_3-water nanofluid flow at a Reynolds number of 1050. Although EMM and EEM models have similar accuracies in prediction of convective heat transfer coefficient, required CPU time for EMM model approximately three times greater than that is required for EEM.

Table 4.5. Computational time [s] comparison of FMC and PC-SIMPLE.

	Eulerian-Eulerian		**Single-phase**	**Eulerian-Mixture**
φ_p[%]	FMC	PC-SIMPLE	SIMPLE	SIMPLE
0.6	82.19	157.14	77.64	552.80
1	89.81	158.62	78.05	572.71
1.6	111.69	163.79	81.68	566.50

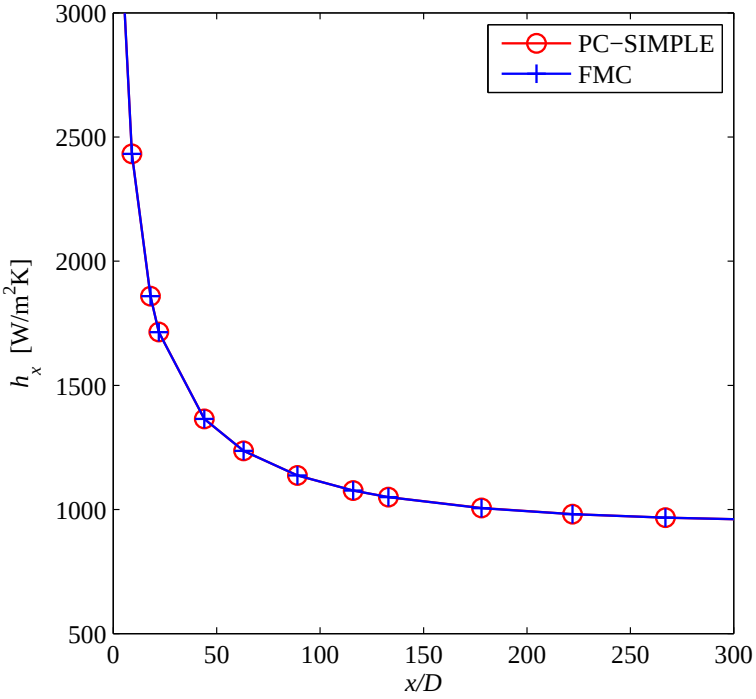

Figure 4.8. Comparison of predicted h_x by PC-SIMPLE and FMC algorithms for 1.6% Al_2O_3-water nanofluid at Re_{nf}=1050.

Although, PC-SIMPLE is a very robust method, it is computationally expensive, since equations are solved in a segregated manner. A remedy might be the use of Full Multiphase Coupled (FMC) scheme for dilute nanofluid systems where equations are solved simultaneously. Figure 4.8 shows that the predicted h_x distributions of FMC and PC-SIMPLE are identical. The complete comparison of models in terms of computational time can be seen in Table 4.5. Overall, the results suggest that computational cost of EEM model can be reduced approximately by 50% while preserving the solution accuracy.

4.4. Hexagonal Boron Nitride Study

So far, single and two phase models have been investigated for modeling of Al_2O_3-water nanofluid by considering their solution accuracies and computational efficiencies. In this section, numerical analysis of laminar forced convection of hexagonal boron nitride-water (hBN-water) nanofluids using, homogeneous single-phase, and two-phase Eulerian-Eulerian models are presented in order to provide numerical data for design

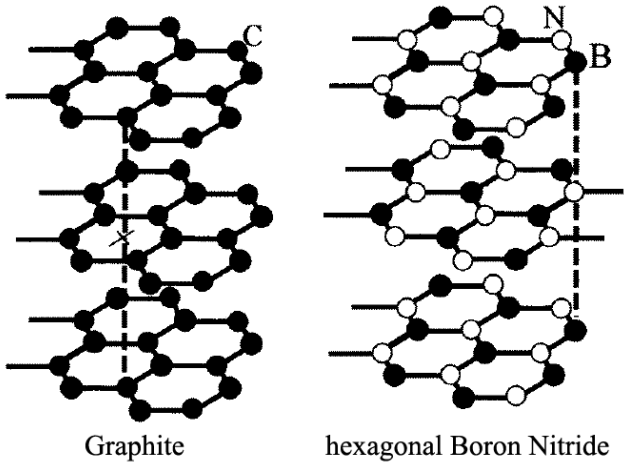

Figure 4.9. Atomic structure of graphite and hexagonal boron nitride. Modified from [77].

of experimental setups for further analysis of hBN-water nanofluids. Since there are no experimental data for calibration, it is not possible to use single phase dispersion and Brownian models for modeling of hBN-water nanofluid.

As stated in previous sections, hBN particles have orthotropic nature due to their atomic structure. As shown in Figure 4.9, they have honeycomb like layered atomic structure [75–77] that is formed by strong covalent bonds. However, since layers are hold together by a weaker Van der Waals bond (slightly ionic), thermal conductivity of hBN differs in perpendicular ($\perp$) and parallel ($\parallel$) directions with respect to its basal plane [77]. The effective thermal conductivity of hBN particles can be estimated by using geometric or arithmetic average of thermal conductivities in these directions. Since there is no exact method presented in the literature, predicted thermal conductivity enhancement for these methods and the directional averaged value given by the manufacturer [37] are compared with experimental data given by Li *et al.* [40]. For specific heat value of hBN, data presented by Ioffe Physical Technical Institute [78] are used. Thermophysical properties of hBN nanoparticles that are used in here, are presented in Table 4.6

In Figure 4.10, predicted thermal conductivity enhancements of hBN-EG nanofluid by Equation 2.4 and the experimental data given by Li *et al.* [40] are compared.

Table 4.6. Physical properties of boron nitride.

	Al_2O_3	hBN
Density [kg/m^3]	3984	2300
Specific Heat [J/Kg K]	755	800
Thermal Conductivity [W/m K]	33	600$\parallel$; 30$\perp$; 33.47(DA)

Since data given by Li *et al.* [40] are the only data in literature for hBN particles, the comparison is based on an ethylene glycol based nanofluid rather than a water based one. The comparison indicates that although the enhancement predicted for all tree effective conductivity values are very close to each other, manufacturer's data and arithmetic average thermal conductivity yield maximum and minimum values, respectively. Therefore, to consider the both extremes, directional averaged (DA) thermal conductivity that is given by the particle's manufacturer [37] and arithmetic average thermal conductivity are used in this study.

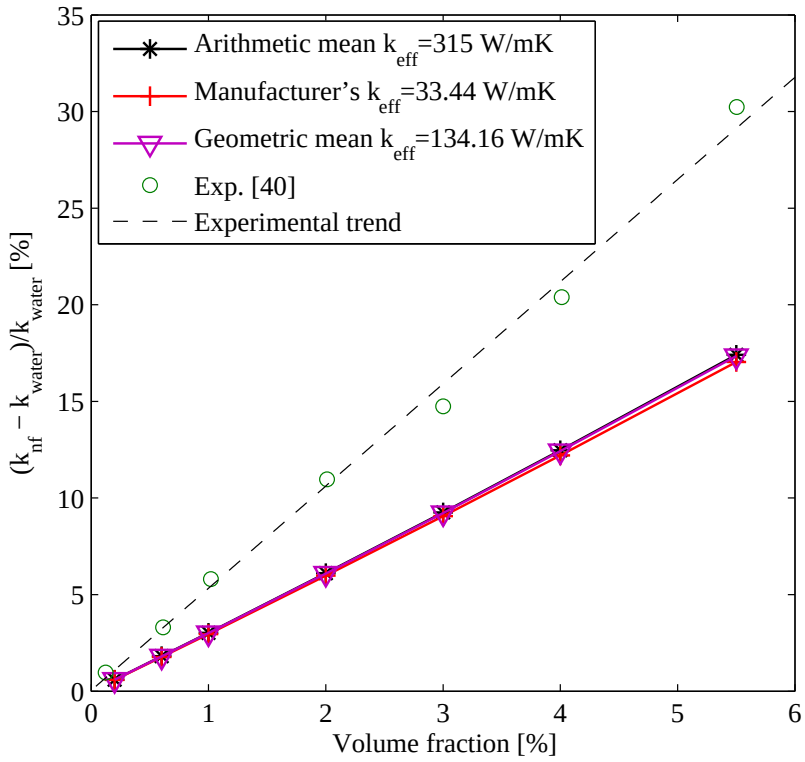

Figure 4.10. Comparison of predicted thermal conductivity enhancement with experimental values.

In Figures 4.11 and 4.12, comparison of convective heat transfer coefficients of hBN-water nanofluid predicted by HSPM and EEM are presented, respectively. In the comparison, particle volume fractions of 0.6%-1.6% are considered for a Reynolds number of 1050. Since no change is observed in thermal conductivity values in Figure 4.10, effective thermal conductivity models are only compared for EEM. The results suggest that the predicted increase in heat transfer coefficient by using the manufacturer's data is very similar to that of Al_2O_3, and the difference between HSPM and EEM is approximately 50%. On the other hand, there is approximately 400% difference between both thermal conductivity models for EEM, and EEM with arithmetic average thermal conductivity predicts 450% increase in heat transfer coefficient. Since there are no available experimental data for comparison, no conclusion can be made on which thermal conductivity method is the best.

However, since the predicted increase exceeds reported values of heat transfer coefficient enhancement in the literature, it can be concluded that non granular EEM might not yield accurate results when used with highly thermally conductive particles.

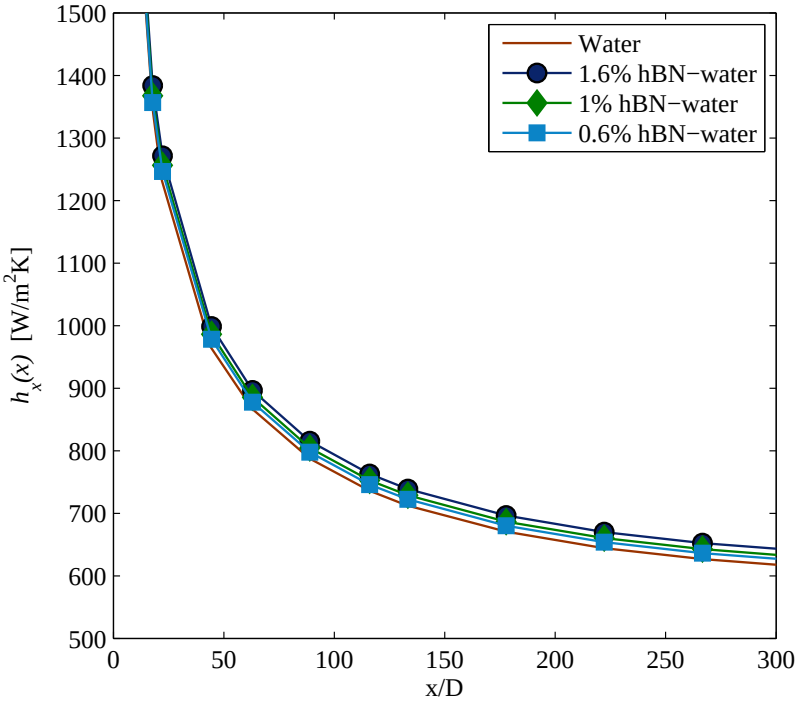

Figure 4.11. Comparison of HSPM results of 0.6%, 1%, and 1.6% hBN-water nanofluid at $Re_{nf} = 1050$.

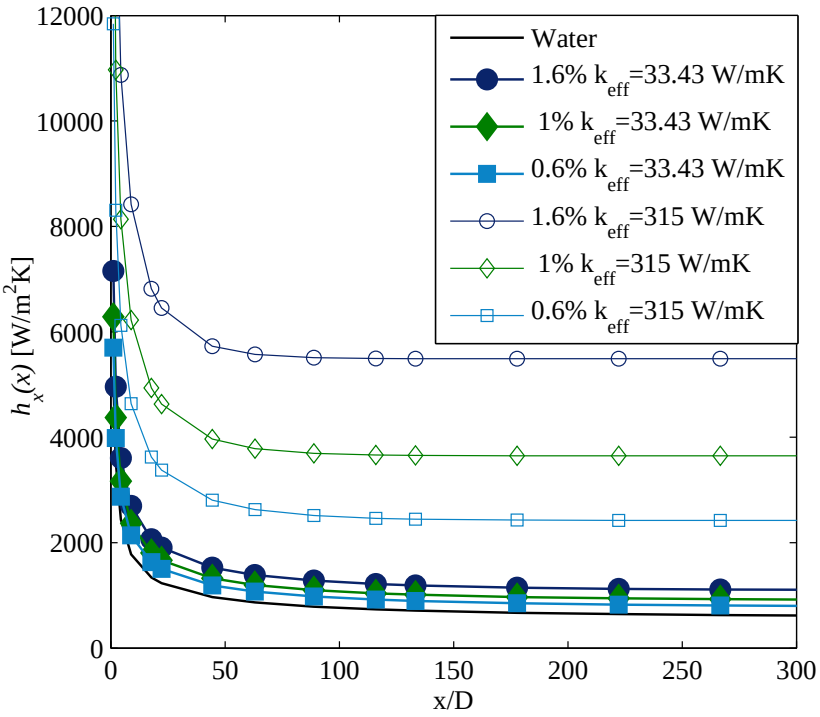

Figure 4.12. Comparison of EEM results of 0.6%, 1%, and 1.6% hBN-water nanofluid at $Re_{nf} = 1050$.

Therefore, although it is a common assumption for two-phase models in literature, non-granular assumption might fail when used with highly thermally conductive particles. However, for a definitive conclusion, results should be compared with experimental results, and EEM model with granular assumption should be investigated.

On the other hand, if data given by the manufacturer are accurate, it can be concluded that since directional averaged thermal conductivity of hBN and Al_2O_3 are very close to each other, experimental comparison of these two nanofluids can help understanding effect of orthotropic nanoparticles on heat transfer of nanofluids.

The friction factor predicted by both models is also compared with Al_2O_3 study, and both EEM and HSPM yields the same results as the Al_2O_3 study. The reason is that in EEM, only physical particle-particle and particle-base fluid interactions such as; collision of particles or drag between phases are taken in to account. Since these interactions are independent of particle type, such a result is expected.

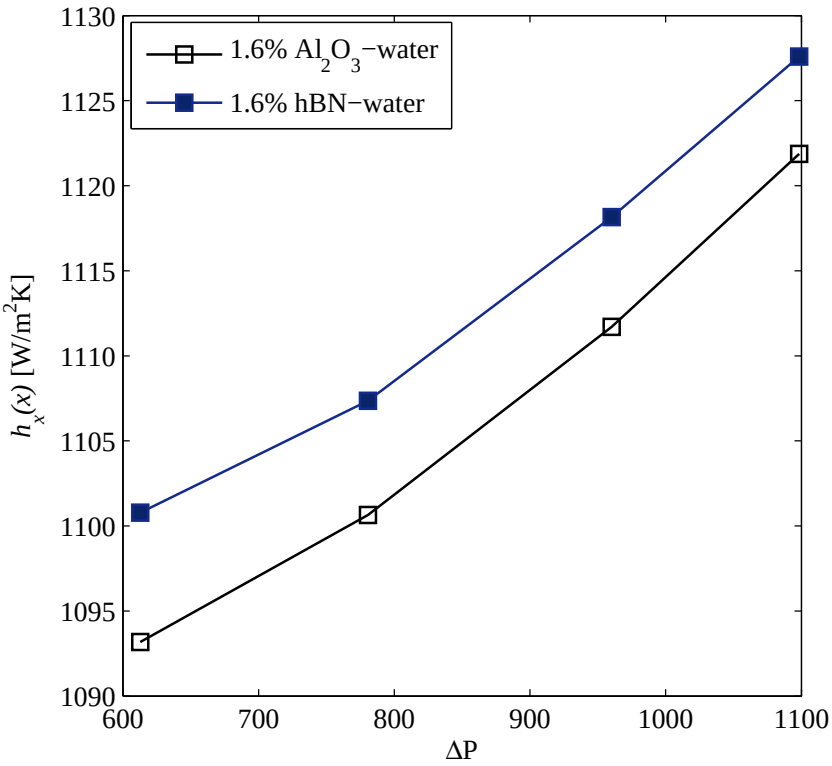

Figure 4.13. Comparison of predicted pressure drop and heat transfer coefficient of hBN and Al_2O_3 water nanofluids by EEM at $Re_{nf} = 1050$.

For a better comparison of hBN and Al_2O_3 water nanofluids, both models are compared in Figure 4.13 by considering predicted convective heat transfer coefficient and pressure drop by EEM with manufacturer's thermal conductivity value. The results suggest that even for the worst case scenario hBN particles enhance heat transfer coefficient better than Al_2O_3 particles at the same pressure drop.

5. SUMMARY AND CONCLUSION

5.1. Summary

In this study, macroscopic modeling of nanofluid flow using single and two phase models are investigated for water based nanofluids. Nanofluid is considered as a single continuum with its effective properties by the single-phase models. Effective properties are calculated by using correlations or theoretical models. Single-phase models that are considered in this study include; homogeneous single-phase, single-phase Brownian, and single-phase dispersion models. In addition to the single-phase models, two-phase Eulerian-Eulerian and Eulerian Mixture models, that consider nanoparticles and base fluids as different continua, are also considered.

First, an extensive literature survey has been carried out on studies that focus on rheology and laminar forced convective of nanofluids. The literature study indicates that there is no study that compares recent state-of-the-art nanofluid models, and single-phase models cannot accurately predict the pressure drop and convective heat transfer coefficient. Furthermore, none of these studies takes computational efficiencies of models in to account while comparing them. Also there is no comparison of computational efficiencies of coupling algorithms that are used in Eulerian-Eulerian two-phase model. It is also observed that Al_2O_3 and other metal oxide particles are the most commonly used nanoparticles in the literature. However, despite their promising physical properties, there are only few studies that focus on characterization of hexagonal boron nitride nanofluids.

To fill these gaps in the literature, homogeneous and non-homogeneous single-phase models together with two-phase Eulerian-Eulerian and Eulerian-Mixture models have been investigated, and a new single-phase dispersion viscosity model is introduced for the first time. Due to availability of data in the literature, Al_2O_3-water nanofluid and the problem domain that is presented by Wen and Ding [24] have been chosen for model validation and development purposes.

First, the homogeneous single-phase model that is presented in Section 2.1 was modeled and compared with experimental studies in the literature. Then, Al_2O_3-water nanofluid have been studied using two-phase Eulerian-Eulerian model. Comparison of both models, and findings in literature indicate that homogeneous single-phase models are not accurate in prediction of heat transfer coefficient and pressure drop compared to two-phase Eulerian-Eulerian model. However, despite being more accurate, two-phase models are found to be computationally expensive compared to single-phase models.

Since a computationally efficient model is a must for design and analysis of commercial products that rely on nanofluids, non-homogeneous single-phase models have been further investigated to increase their prediction accuracies. During the study, single-phase Brownian and dispersion models have been investigated, and a new dispersion viscosity model was proposed for increased solution accuracy of single-phase models. Results suggest that single-phase dispersion model presented by Mokmeli and Saffar-Avval [27], and the dispersion viscosity model that is presented by this study are the most accurate single-phase models in prediction of convective heat transfer coefficient and pressure drop, respectively. However, it is also observed that these models cannot be used, if there are no experimental data for calibration.

To provide a comparison of recent state-of-the-art single and two phase nanofluid models, homogeneous and non-homogeneous single-phase models presented in Section 2.1, and two-phase models presented in Section 2.2 are compared in terms of their computational efficiency and solution accuracy. Furthermore for Eulerian-Eulerian model, solution accuracy and computational efficiency of two different coupling algorithms are compared. The results of these studies are discussed in Chapter 4. Overall, results suggest that the most effective single and two phase models are single-phase dispersion viscosity and two-phase Eulerian-Eulerian models, respectively. Results also show that computational efficiency of Eulerian-Eulerian model can be increased up to 50%, by use of Full Multiphase Coupled scheme as a coupling algorithm.

Finally, to provide numerical data for design of experimental setups, hBN-water nanofluids have been investigated using homogeneous single-phase and Eulerian-Eu-

lerian two-phase models. Since there have not been any experimental data regarding the forced convection and effective thermal conductivity of hBN-water nanofluid, the results only compared between single and two phase models.

5.2. Conclusion

Single and two-phase models have been investigated for the characterization of laminar forced convection of Al_2O_3-water nanofluid with various particle volume fractions in a circular tube. Single-phase thermal dispersion model suggested by Mokmeli and Saffar-Avval [27] is found to be the most accurate single-phase model in prediction of convective heat transfer coefficient. This model is recommended for applications, when calibration data is available, thermal analysis is the objective, and computational efficiency is important. Furthermore, it is shown that for Reynolds numbers and particle volume fractions considered in this study, calibration constant used in the definition of dispersion conductivity model is independent of Reynolds number and volume fraction of particles. Therefore, the model can be used at varying Reynolds numbers and particle volume fractions without any re-calibration. It is also observed that Eulerian-Eulerian and Eulerian-Mixture models under predict heat transfer coefficient at the beginning of the entry region then, as the flow develops both models start to over predict the heat transfer coefficient. Considering its computational efficiency, Eulerian-Eulerian two-phase model is recommended for applications, when no prior experimental data are available, and prediction of both heat transfer and pressure drop is important. It is also showed that for the Eulerian-Eulerian two phase model, computational cost can be reduced approximately 50% by using Full Multiphase Coupled algorithm without sacrificing solution accuracy.

Comparison of Al_2O_3-water results with hexagonal boron nitride results, it is evident that single phase models have limited capacity, if there are no experimental data available for model calibration. Furthermore, it is observed that non-granular assumption might not be valid for highly thermally conductive particles, and granular models should be investigated. Results also suggest that at a fixed pressure drop, hBN particles enhance heat transfer coefficient more compared to Al_2O_3 particles.

5.3. Suggestions for Future Studies

At the moment, many of the studies in literature consider steady state analysis of nanofluids using macroscopic models. The results suggest that there is no significant difference between two-phase models in terms of prediction accuracy of convective heat transfer coefficient at steady state. Therefore, unsteady analysis of models may shed light on differences between single and two phase models and help to understand interactions between particles and base fluid.

Results suggest that single-phase dispersion model is the most accurate single-phase model. However in literature, it is observed that there is a lack of data for calibration constants of different nanofluids. An extensive study that includes dispersion model calibration constants for different nanoparticles and base fluids would be a great asset for single-phase models. Existence of such data would ease use of dispersion models in design and analysis of equipment that use nanofluids.

Considering results of the hexagonal boron nitride (hBN) study, there are few experimental data about forced convection and thermal conductivity of hBN nanofluids. Although orthotropy of hBN participles can be seen as a major drawback at first glance, if such particles can be manipulated by an external force field, properties of the nanofluid can be altered without changing its composition. Moreover, micro or nanoscale heat valves can be designed using an isotropic nanoparticles. Therefore, experimental studies that would help understanding effect of anisotropy on nanofluid properties would be a great asset for the nanofluid literature.

Literature review on two-phase models revealed that, all of the two-phase models that are used in nanofluid modeling, are based on macroscopic models. Therefore, studies that focus on modeling and understanding of phase interactions for nanofluids would enhance prediction accuracies of two-phase models.

APPENDIX A: USER DEFINED FUNCTIONS

Codes for User Defined Functions (UDF) that are used in definition of models and material properties in FLUENT are presented here.

A.1. Single-phase Dispersion Model #1

```
/*This UDF calculates temperature dependent thermal conductivity of
Al2O3-water nanofluid using thermal dispersion model.*/
/*model: SPD1
/*Code by: Sinan GÖKTEPE
/*Ver:2.1
/*Last modif: 02.05.2012
/*Units: ALL IS [m, K, kg, s]*/

/*##############################################*/
/* ALL UNITS ARE I.S. USE KELVIN FOR TEMPERATURE*/
/*##############################################*/
#include "udf.h"
#define Cp_bf 4182 /*Cp of Water*/
#define k_bf 0.6 /*BaseFluid Conductivity*/
#define rho_bf 998 /*Basefluid density*/
#define alpha 0.143E-6 /*Thermal Diffusivity of Water*/
#define d_bf 0.29E-9 /*Diameter of water molecule*/
#define l_bf 0.17E-9 /*Mean free path of water molecules*/

#define d_p 45E-9 /*Nanoparticle Size*/
#define vof 0.006 /*Volume fraction of Al2O3*/
#define k_p 33 /*Conductivity of Al2O3*/
#define rho_al2o3 3984          /*Density of Al2O3*/
#define Cp_al2o3 755 /*Cp of Al2O3*/
```

```
#define pi 3.14159265359        /*Pi Number*/
#define CC 2.15E+5      /*Thermal dispersion constant*/
#define r 0.00225 /*Radius of Pipe [m] */

/* Definition of Temperature Dependent Conductivity*/
DEFINE_PROPERTY(k_dispersion,cell,thread)
{
  real ktc;
  real Re;
  real Pr;
  real mu;
  real kd;
  real ux;
  real ktc_eff;
  real rho_nf = rho_bf*(1-vof)+rho_al2o3*vof;
  real Cp_nf =  Cp_bf*(1-vof)+Cp_al2o3*vof;
  real temp = C_T(cell,thread);  /*Read cell temperature*/
  mu = A*pow(10,B/(temp-C));
  Pr = mu/(rho_bf*alpha);
  Re = rho_bf*k_b*temp/(3*pi*pow(mu,2)*l_bf);
  ktc = k_bf*(1+64.7*pow(vof,0.7460)*pow((d_bf/d_p),0.3690)...
 ...*pow((k_p/k_bf),0.7476)*pow(Pr,0.9955)*pow(Re,1.2321));...
 .../*conductivity function*/
  /*---------------- Dispersion ------------------*/

  ux =  C_U(cell,thread);          /*Read velocity*/
  kd = CC*rho_nf*Cp_nf*ux*vof*d_p*r;
  ktc_eff = kd+ktc;
  return (ktc_eff);
}
```

```
/*End of Conductiviy*/
```

A.2. Single-phase Dispersion Model #2

```
/*This UDF calculates temperature dependent thermal conductivity
of Al2O3-water nanofluid using thermal dispersion model.*/
/*model: SPD2
/*Code by: Sinan GÖKTEPE
/*Ver:2.4
/*Last modif: 02.05.2012
/*Units: ALL IS [m, K, kg, s]*/

/*##############################################*/
/* ALL UNITS ARE I.S. USE KELVIN FOR TEMPERATURE*/
/*##############################################*/

#include "udf.h"

#define Cp_bf 4182 /*Cp of Water*/
#define k_bf 0.6 /*BaseFluid Conductivity*/
#define rho_bf 998 /*Basefluid density*/
#define alpha 0.143E-6 /*Thermal Diffusivity of Water*/
#define d_bf 0.29E-9 /*Diameter of water molecule*/
#define l_bf 0.17E-9 /*Mean free path of water molecules*/

#define d_p 45E-9 /*Nanoparticle Size*/
#define vof 0.006 /*Volume fraction of Al2O3*/
#define k_p 33 /*Conductivity of Al2O3*/
#define rho_al2o3 3984          /*Density of Al2O3*/
#define Cp_al2o3 755 /*Cp of Al2O3*/
```

```
#define CC -2E-13 /*Thermal dispersion constant for al2o3-di-water*/

#define r 0.00225 /*Radius of Pipe [m] */

/* Definition of Temperature Depentdent Conductivity*/
DEFINE_PROPERTY(k_dispersion,cell,thread)
{
  real ktc;
  real Re;
  real Pr;
  real mu;
  real kd;
  real dr_ux;
  real ktc_eff;
  real rho_nf = rho_bf*(1-vof)+rho_al2o3*vof;
  real Cp_nf =  Cp_bf*(1-vof)+Cp_al2o3*vof;
  real temp = C_T(cell,thread);  /*Read cell temperature*/
  mu = A*pow(10,B/(temp-C));
  Pr = mu/(rho_bf*alpha);
  Re = rho_bf*k_b*temp/(3*pi*pow(mu,2)*l_bf);
  ktc = k_bf*(1+64.7*pow(vof,0.7460)*pow((d_bf/d_p),0.3690)*...
  ...pow((k_p/k_bf),0.7476)*pow(Pr,0.9955)*pow(Re,1.2321));...
 ... /*conductivity function*/
  /*---------------- Dispersion ------------------*/

  dr_ux =  C_U_G(cell,thread)[1];
  kd = CC*rho_nf*Cp_nf*dr_ux*vof*r/d_p;
  ktc_eff = kd+ktc;
  return (ktc_eff);
}
/*End of Conductiviy*/
```

A.3. Single-phase Brownian Viscosity Model

```
/*This UDF calculates temperature dependent thermal conductivity
of Al2O3-water nanofluid using Brownian thermal conductivity model.*/
/*model: SPBM
/*Code by: Sinan GÖKTEPE
/*Ver:2.4
/*Last modif: 02.05.2012
/*Units: ALL IS [m, K, kg, s]*/
/*#########################################################*/
/*    ALL UNITS ARE I.S. USE KELVIN FOR TEMPERATURE
/*#########################################################*/

#include "udf.h"

#define phi 0.006 /*Volume fraction of Al2O3*/
#define k_p 33   /*Conductivity of Al2O3*/
#define rho_p 3984              /*Density of Al2O3*/
#define Cp_p 755     /*Cp of Al2O3*/

#define rho_bf 998              /*Density of H2O*/
#define Cp_bf 4181  /*at 25oC */
#define k_bf  0.6096            /*at 300K from NIST*/
#define mu_bf 0.7978E-3 /*at 300K from NIST*/

#define boltzmann 1.3807E-23 /*Boltzamn constant*/
#define pi 3.14159265359                /*Pi Number*/
#define D 4.5E-3           /*Diameter of Pipe [m] */

/*Definition of Brownian Visocsity*/
DEFINE_PROPERTY(k_brownian,cell,thread)
{
```

```
real k_static=k_bf*(1+(3*(k_p/k_bf-1)*phi)/(k_p/k_bf+2...
...-(k_p/k_bf-1)*phi));/*Maxwell Formualation*/
real Cp_nf=((1-phi)*rho_bf*Cp_bf+phi*rho_p*Cp_p)/...
...((1-phi)*rho_bf+phi*rho_p);
real T = C_T(cell,thread);
real beta=0.0017*pow((100*phi),-0.0841);
real f=(-0.8467*phi+0.0753)*T+(237.67*phi-21,998);
real k_brownian=5E4*beta*phi*rho_p*Cp_p*...
...sqrt(boltzmann*T/(rho_p*D))*f;
real k_app=k_static+k_brownian;
return(k_app);
}
/*end  of definition*/
```

A.4. Single-phase Brownian Viscosity Model

```
/*This UDF calculates brownian viscosity of alo3-water nanofluid
/*model: BVM
/*Code by: Sinan GÖKTEPE
/*Ver:2.1
/*Last modif: 02.05.2012
/*Units: ALL IS [m, K, kg, s]*/
/*############################################################*/
/*    ALL UNITS ARE I.S. USE KELVIN FOR TEMPERATURE       */
/*############################################################*/

#include "udf.h"

#define phi 0.003 /*Volume fraction of Al2O3*/

#define k_p 33   /*Conductivity of Al2O3*/
```

```
#define rho_p 3984              /*Density of Al2O3*/
#define Cp_p 755     /*Cp of Al2O3*/

#define rho_bf 998              /*Density of H2O3*/
#define Cp_bf 4181  /*at 25oC */
#define k_bf  0.6096            /*at 300K from NIST*/

#define boltzmann 1.3807E-23 /*Boltzamn constant*/
#define pi 3.14159265359                /*Pi Number*/

#define D 4.5E-3           /*Diameter of Pipe [m] */
#define mu_bf 0.001003 /*Basefluid visco

/*Definition of Brownian Visocsity*/
DEFINE_PROPERTY(mu_brownian,cell,thread)
{
real Cp_nf=((1-phi)*rho_bf*Cp_bf+phi*rho_p*Cp_p)/...
...((1-phi)*rho_bf+phi*rho_p);
real T = C_T(cell,thread);
real beta=0.0017*pow((100*phi),-0.0841);
real f=(-0.8467*phi+0.0753)*T+(237.67*phi-21.998);
real k_brownian=5E4*beta*phi*rho_p*Cp_p*sqrt(boltzmann*T/...
...(rho_p*D))*f;
real mu_static=(1+2.5*phi)*mu_bf;
real mu_brownian=k_brownian/Cp_nf;
real mu_nf=mu_static+mu_brownian;
return (mu_nf);
}

/*Thermal COnd*/
DEFINE_PROPERTY(k_brownian,cell,thread)
```

```
{
real k_static=k_bf*(1+(3*(k_p/k_bf-1)*phi)/(k_p/k_bf+2-...
...(k_p/k_bf-1)*phi));/*Maxwell Formualation*/
real Cp_nf=((1-phi)*rho_bf*Cp_bf+phi*rho_p*Cp_p)/...
...((1-phi)*rho_bf+phi*rho_p);
real T = C_T(cell,thread);
real beta=0.0017*pow((100*phi),-0.0841);
real f=(-0.8467*phi+0.0753)*T+(237.67*phi-21.998);
real k_brownian=5E4*beta*phi*rho_p*Cp_p*sqrt(boltzmann*T/(rho_p*D))*f;
real k_app=k_static + k_brownian;
return(k_app);
}
```

A.5. Single-phase Dispersion Viscosity Model

```
/*This UDF calculates dispersion viscosity and conductivity
of Al2O3-water nanofluid based on Mokmeli et al.
/*model: DVM
/*Code by: Sinan GÖKTEPE
/*Ver:2.4
/*Last modif: 02.05.2012
/*Units: ALL IS [m, K, kg, s]*/
/*BEFORE EXECUTE, YOU MUST ENABLE STORAGE OF GRADIENTS IN FLUENT BY */
/*solve/expert/keep cell residuals from being freed*/

/*############################################*/
/* ALL UNITS ARE IS USE KELVIN FOR TEMPERATURE*/
/*############################################*/

#include "udf.h"
```

```
#define Cp_bf 4182 /*Cp of Water*/
#define k_bf 0.6 /*BaseFluid Conductivity*/
#define rho_bf 998 /*Basefluid density*/
#define alpha 0.143E-6 /*Thermal Diffusivity of Water*/
#define d_bf 0.29E-9 /*Diameter of water molecule*/
#define l_bf 0.17E-9 /*Mean free path of water molecules*/

#define d_p 45E-9 /*Nanoparticle Size*/
#define vof 0.003 /*Volume fraction of Al2O3*/
#define k_p 33 /*Conductivity of Al2O3*/
#define rho_al2o3 3984          /*Density of Al2O3*/
#define Cp_al2o3 755 /*Cp of Al2O3*/

#define k_b 1.3807E-23 /*Boltzamn constant*/
#define pi 3.14159265359        /*Pi Number*/
#define A 2.414E-5 /*Correlation Constant*/
#define B 247.8 /*Correlation Constant*/
#define C 140 /*Correlation Constant*/
#define CC -2E-13 /*Thermal dispersion constant for al2o3-di-water*/

#define r 0.00225 /*Radius of Pipe [m] */

/* Definition of Temperature Dependent Conductivity*/
DEFINE_PROPERTY(k_dispersion,cell,thread)
{
  real ktc;
  real Re;
  real Pr;
  real mu;
  real kd;
  real dr_ux;
```

```
  real ktc_eff;
  real rho_nf = rho_bf*(1-vof)+rho_al2o3*vof;
  real Cp_nf =  Cp_bf*(1-vof)+Cp_al2o3*vof;
  real temp = C_T(cell,thread);  /*Read cell temperature*/
  mu = A*pow(10,B/(temp-C));
  Pr = mu/(rho_bf*alpha);
  Re = rho_bf*k_b*temp/(3*pi*pow(mu,2)*l_bf);
  ktc = k_bf*(1+64.7*pow(vof,0.7460)*pow((d_bf/d_p),0.3690)
  *pow((k_p/k_bf),0.7476)*pow(Pr,0.9955)*pow(Re,1.2321));...
  ...  /*conductivity function*/
  /*---------------- Dispersion ------------------*/

  dr_ux =  C_U_G(cell,thread)[1];
  kd = CC*rho_nf*Cp_nf*dr_ux*vof*r/d_p;
  ktc_eff = kd+ktc;
  return (ktc_eff);
}
/*End of Conductiviy*/

/* Definition of Brownian Viscosit*/
DEFINE_PROPERTY(mu_dispersion,cell,thread)
{
  real rho_nf = rho_bf*(1-vof)+rho_al2o3*vof;   /*Define rho_nf*/
  real Cp_nf =  Cp_bf*(1-vof)+Cp_al2o3*vof;     /*Define Cp_nf*/
  real temp = C_T(cell,thread);     /*Read cell temperature*/

  real dr_ux =  C_U_G(cell,thread)[1];     /*Read cell gradient*/
  real kd = CC*rho_nf*Cp_nf*dr_ux*vof*r/d_p;  /*define dispersion...
  ...conductivity, ref: Mokmeli*/
  real mu_d=kd/Cp_nf;  /*define dispersion viscosity*/
  real mu_static=(1+2.5*vof)*0.001003;
```

```
  real mu_eff=mu_static+mu_d;
  return (mu_eff);
}
```

APPENDIX B: USER GUIDE

The purpose of this user guide is to provide users a guidance to under stand the model and file structure used in the study. Some additional helpful tips about setting up and running the ANSYS 13.0 Workbench and FLUENT are also provided.

B.1. System Configuration

This model is created under a 64bit machine operating on Microsoft Windows 7. If not done before, some required changes must be done by the user in order to use UDFs in FLUENT. Following steps are required, if FLUENT gives 'missing nmake' error message. This setup process is summarized from the CFD online.

(i) Install Visual C++ 2008 Express Edition or a newer version.

(ii) Set the correct environment variables in ''System variables" section as;

C:\...\Microsoft Visual Studio 10.0\Common7\Tools;

C:\...\Microsoft Visual Studio 10.0\VC\bin;

C:\...\ANSYS Inc\v120\fluent\ntbin\win64.

(iii) Install a Software Development Kit (SKD) for 64bit systems.

(iv) Launch FLUENT from the SDK command prompt (not from the Windows command prompt).

B.2. Job Scheduling

Scheduling jobs can save great deal of time, if it is done properly. Depending on size and requirements of the study this process should be carefully evaluated by the user since, an improper setup may lead to increased computational time. Here, basics of job scheduling by using ANSYS Remote Solve Manger (RSM) is outlined.

First, user must set up and install prerequisites and RSM as described in ANSYS User Manual. Then, frequently varying variables should be selected, and parameters

Table B.1. File names and corresponding models.

Model name	Model	File name	Nanofluid
HSPM	Single-phase	SP_Hamilton_Circ2D_Wen.wbpj	Al_2O_3-water
HSPM-TD	Single-phase	SP_Hamilton_Circ2D_Wen.wbpj	Al_2O_3-water
SPBM	Single-phase	brownian_mod.wbpj	Al_2O_3-water
SPDM	Single-phase	SP_Hamilton_Circ2D_Wen.wbpj	Al_2O_3-water
EEM	Two-phase	Circular_Eulerian-eulerian_2.wbpj	Al_2O_3-water
EMM	Two-phase	Circular_Mixture_2.wbpj	Al_2O_3-water
EEM	Two-phase	EEM-CBN.wbpj	CBN/hBN-water
HSPM	Single-phase	cbn-sp.wbpj	CBN/hBN-water
DVM	Single-phase	Visco_Sub.wbpj	CBN/hBN-water
BVM	Single-phase	Visco_Sub.wbpj	CBN/hBN-water

should be assigned to those variables in corresponding environment (FLUENT, Design Modeler, etc.). Now, in the Workbench environment, range of variables can be submitted into one FLUENT case to be solved conservatively. Such approach is suggested for simple systems that does not contain many components. For the large systems, each case should be considered in a different cell. After setting up a single cell, other cells can be easily set by duplicating the mother cell and changing its parameters from the parameters window in Workbench. Now one can click "Update Project" and let the Workbench get each case solved to FLUENT via RSM.

In Table B.1 models and corresponding file names are provided. Files ending with *dp*.wbpj should be neglected and all models must be run from the file name described in the table. If a UDF required for the model, it is included in the model folder, and no action required by the user. For more detailed explanation about file structure, one should refer to ANSYS User Guide.

REFERENCES

1. Sarkar, J., "A Critical Review on Convective Heat Transfer Correlations of Nanofluids", *Renewable and Sustainable Energy Reviews*, Vol. 15, No. 6, pp. 3271–3277, 2011.

2. Choi, S. U. and J. Eastman, "Enhancing Thermal Conductivity of Fluids with Nanoparticles", Tech. rep., Argonne National Lab., IL (United States), 1995.

3. Keblinski, P., S. Phillpot, S. Choi and J. Eastman, "Mechanisms of Heat Flow in Suspensions of Nano-sized Particles (nanofluids)", *International Journal of Heat and Mass Transfer*, Vol. 45, No. 4, pp. 855 – 863, 2002.

4. Sridhara, V. and L. N. Satapathy, "Al_2O_3-based Nanofluids: A Review", *Nanoscale Research Letters*, Vol. 6, No. 1, pp. 1–16, 2011.

5. Godson, L., B. Raja, D. Mohan Lal and S. Wongwises, "Enhancement of Heat Transfer Using Nanofluids—an Overview", *Renewable and Sustainable Energy Reviews*, Vol. 14, No. 2, pp. 629–641, 2010.

6. Yu, W., D. M. France, S. U. Choi and J. L. Routbort, "Review and Assessment of Nanofluid Technology for Transportation and other Applications", Tech. Rep. 1, Argonne National Laboratory, Chicago, IL, April 2007.

7. Saidur, R., K. Leong and H. Mohammad, "A Review on Applications and Challenges of Nanofluids", *Renewable and Sustainable Energy Reviews*, Vol. 15, No. 3, pp. 1646–1668, 2011.

8. Natarajan, E. and R. Sathish, "Role of Nanofluids in Solar Water Heater", *The International Journal of Advanced Manufacturing Technology*, 2009.

9. Tzeng, S., C. Lin and K. Huang, "Heat Transfer Enhancement of Nanofluids in Rotary Blade Coupling of Four-wheel-drive Vehicles", *Acta Mechanica*, Vol. 179, No. 1-2, pp. 11–23, 2005.

10. Jang, S. P. and S. U. Choi, "Analysis of Microchannel Heat Sink Performance Using Nanofluids", *Applied Thermal Engineering*, Vol. 25, No. 17–18, pp. 3104–3114, 2005.

11. Jang, S. P. and S. U. Choi, "Cooling Performance of a Microchannel Heat Sink with Nanofluids", *Applied Thermal Engineering*, Vol. 26, No. 17–18, pp. 2457–2463, 2006.

12. Chein, R. and J. Chuang, "Experimental Microchannel Heat Sink Performance Studies Using Nanofluids", *International Journal of Thermal Sciences*, Vol. 46, No. 1, pp. 57 – 66, 2007.

13. Tsai, C., H. Chien, P. Ding, B. Chan, T. Luh and P. Chen, "Effect of Structural Character of Gold Nanoparticles in Nanofluid on Heat Pipe Thermal Performance", *Materials Letters*, Vol. 58, No. 9, pp. 1461–1465, 2004.

14. Chien, H. T., C. I. Tsai, P. H. Chen and P. Y. Chen, "Improvement on Thermal Performance of a Disk-shaped Miniature Heat Pipe with Nanofluid", *Electronic Packaging Technology Proceedings*, pp. 389–391, October 2003.

15. Shima, P. and J. Philip, "Tuning of Thermal Conductivity and Rheology of Nanofluids Using an External Stimulus", *The Journal of Physical Chemistry C*, Vol. 115, No. 41, pp. 20097–20104, 2011.

16. Lajvardi, M., J. Moghimi Rad, I. Hadi, A. Gavili, T. Dallali Isfahani, F. Zabihi and J. Sabbaghzadeh, "Experimental Investigation for Enhanced Ferrofluid Heat Transfer Under Magnetic Field Effect", *Journal of Magnetism and Magnetic Materials*, Vol. 322, No. 21, pp. 3508 – 3513, 2010.

17. Hong, H., B. Wright, J. Wensel, S. Jin, X. R. Ye and W. Roy, "Enhanced Thermal Conductivity by the Magnetic Field in Heat Transfer Nanofluids Containing Carbon Nanotube", *Synthetic Metals*, Vol. 157, No. 10–12, pp. 437 – 440, 2007.

18. Zeinali Heris, S., S. G. Etemad and M. Nasr Esfahany, "Experimental Investigation of Convective Heat Transfer of Al_2O_3/water Nanofluid in Circular Tube", *International Journal of Heat and Fluid Flow*, Vol. 28, No. 2, pp. 203 – 210, 2007.

19. Pak, B. C. and Y. I. Cho, "Experiments to Explore the Mechanisms of Heat Transfer in Nanocrystalline Alumina/water Nanofluid Under Laminar and Turbulent Flow Conditions", *Experimental Heat Transfer*, Vol. 11, No. 2, pp. 151–170, 1998.

20. Sommers, A. and K. Yerkes, "Experimental Investigation into the Convective Heat Transfer and System-level Effects of Al_2O_3-propanol Nanofluid", *Journal of Nanoparticle Research*, Vol. 12, pp. 1003–1014.

21. Xuan, Y. and Q. Li, "Heat Transfer Enhancement of Nanofluids", *International Journal of Heat and Fluid Flow*, Vol. 21, No. 1, pp. 58–64, 2000.

22. Maiga, S. E. B., C. T. Nguyen, N. Galanis and G. Roy, "Heat Transfer Behaviours of Nanofluids in a Uniformly Heated Tube", *Superlattices and Microstructures*, Vol. 35, No. 3, pp. 543–557, 2004.

23. Haghshenas Fard, M., M. N. Esfahany and M. Talaie, "Numerical Study of Convective Heat Transfer of Nanofluids in a Circular Tube Two-phase Model versus Single-phase Model", *International Communications in Heat and Mass Transfer*, Vol. 37, No. 1, pp. 91–97, 2010.

24. Wen, D. and Y. Ding, "Experimental Investigation into Convective Heat Transfer of Nanofluids at The Entrance Region Under Laminar Flow Conditions", *International Journal of Heat and Mass Transfer*, Vol. 47, No. 24, pp. 5181 – 5188, 2004.

25. Bianco, V., F. Chiacchio, O. Manca and S. Nardini, "Numerical Investigation of Nanofluids Forced Convection in Circular Tubes", *Applied Thermal Engineering*, Vol. 29, No. 17–18, pp. 3632 – 3642, 2009.

26. Akbari, M., N. Galanis and A. Behzadmehr, "Comparative Analysis of Single and Two-phase Models for CFD Studies of Nanofluid Heat Transfer", *International Journal of Thermal Sciences*, Vol. 50, No. 8, pp. 1343–1354, 2011.

27. Mokmeli, A. and M. Saffar-Avval, "Prediction of Nanofluid Convective Heat Transfer Using the Dispersion Model", *International Journal of Thermal Sciences*, Vol. 49, No. 3, pp. 471–478, 2010.

28. Kalteh, M., A. Abbassi, M. Saffar-Avval and J. Harting, "Eulerian–Eulerian Two-phase Numerical Simulation of Nanofluid Laminar Forced Convection in a Microchannel", *International Journal of Heat and Fluid Flow*, Vol. 32, No. 1, pp. 107 – 116, 2011.

29. Anoop, K., T. Sundararajan and S. K. Das, "Effect of Particle Size on the Convective Heat Transfer in Nanofluid in the Developing Region", *International Journal of Heat and Mass Trasnfer*, Vol. 52, 2009.

30. Özerinç, S., A. Yazıcıoğlu and S. Kakaç, "Numerical Analysis of Laminar Forced Convection with Temperature-dependent Thermal Conductivity of Nanofluids and Thermal Dispersion", *International Journal of Thermal Sciences*, Vol. 62, pp. 138 – 148, 2012.

31. Mirmasoumi, S. and A. Behzadmehr, "Numerical Study of Laminar Mixed Convection of a Nanofluid in a Horizontal Tube Using Two-phase Mixture Model", *Applied Thermal Engineering*, Vol. 28, No. 7, pp. 717–727, 2008.

32. Hwang, K. S., S. P. Jang and S. U. Choi, "Flow and Convective Heat Transfer Characteristics of Water-based Al_2O_3 Nanofluids in Fully Developed Laminar Flow Regime", *International Journal of Heat and Mass Transfer*, Vol. 52, No. 1–2, pp. 193 – 199, 2009.

33. Raisee, M. and M. Moghaddami, "Numerical Investigation of Laminar Forced Convection of Nanofluids Through Circular Pipes", *Journal of Enhanced Heat Transfer*, Vol. 15, No. 4, 2008.

34. Anoop, K., S. Kabelac, T. Sundararajan and S. K. Das, "Rheological and Flow Characteristics of Nanofluids: Influence of Electroviscous Effects and Particle Agglomeration", *Journal of Applied Physics*, Vol. 106, No. 3, 2009.

35. Lotfi, R., Y. Saboohi and A. Rashidi, "Numerical Study of Forced Convective Heat Transfer of Nanofluids: Comparison of Different Approaches", *International Communications in Heat and Mass Transfer*, Vol. 37, No. 1, pp. 74–78, 2010.

36. Wang, X. Q. and A. S. Mujumdar, "A Review on Nanofluids-part I: Theoretical and Numerical Investigations", *Brazilian Journal of Chemical Engineering*, Vol. 25, No. 4, pp. 613–630, 2008.

37. "Hexagonal Boron Nitride (hBN) Powder", 2008, http://www.lowerfriction.com-/pdf/11.pdf, accessed at May 2013.

38. "BN - Boron Nitride Electrical Properties", 2001, http://www.ioffe.ru/SVA/-NSM/Semicond/BN/ebasic.html, accessed at May 2013.

39. Solozhenko, V. and T. Peun, "Compression and Thermal Expansion of Hexagonal Graphite-like Boron Nitride up to 7 GPa and 1800 K", *Journal of Physics and Chemistry of Solids*, Vol. 58, No. 9, pp. 1321–1323, 1997.

40. Li, Y., J. Zhou, Z. Luo, S. Tung, E. Schneider, J. Wu and X. Li, "Investigation on Two Abnormal Phenomena about Thermal Conductivity Enhancement of BN/EG Nanofluids", *Nanoscale Research Letters*, Vol. 6, No. 1, p. 443, 2011.

41. Göktepe, S., K. Atalık and H. Ertürk, "Assessment of Single and Two-phase Models for Nanofluid Flow at the Entrance Region of a Uniformly Heated Tube", *International Mehcanical Engineering Congress and Exhibiton, Houston, TX*, 86274, ASME, November 2012.

42. Ghadimi, A., R. Saidur and H. Metselaar, "A Review of Nanofluid Stability Properties and Characterization in Stationary Conditions", *International Journal of Heat and Mass Transfer*, Vol. 54, No. 17, pp. 4051–4068, 2011.

43. Ding, Y., H. Chen, Z. Musina, Y. Jin, T. Zhang, S. Witharana and W. Yang, "Relationship Between the Thermal Conductivity and Shear Viscosity of Nanofluids", *Physica Scripta*, Vol. 2010, No. T139, 2010.

44. Wang, X., X. Xu and S. U. S. Choi, "Thermal Conductivity of Nanoparticle-fluid Mixture", *Journal of Thermophysics and Heat Transfer*, Vol. 13, No. 4, pp. 474–480, 1999.

45. Das, S. K., N. Putra and W. Roetzel, "Pool Boiling Characteristics of Nano-fluids", *International Journal of Heat and Mass Transfer*, Vol. 46, No. 5, pp. 851–862, 2003.

46. Chen, H., Y. Ding and C. Tan, "Rheological Behaviour of Nanofluids", *New Journal of Physics*, Vol. 9, No. 10, p. 367, 2007.

47. He, Y., Y. Jin, H. Chen, Y. Ding, D. Cang and H. Lu, "Heat Transfer and Flow Behaviour of Aqueous Suspensions of TiO_2 Nanoparticles (nanofluids) Flowing Upward Through a Vertical Pipe", *International Journal of Heat and Mass Transfer*, Vol. 50, No. 11, pp. 2272–2281, 2007.

48. Murshed, S., K. Leong and C. Yang, "Investigations of Thermal Conductivity and Viscosity of Nanofluids", *International Journal of Thermal Sciences*, Vol. 47, No. 5, pp. 560–568, 2008.

49. Ding, Y., H. Chen, Y. He, A. Lapkin, M. Yeganeh, L. Siller and Y. V. Butenko, "Forced Convective Heat Transfer of Nanofluids", *Advanced Powder Technology*, Vol. 18, No. 6, pp. 813–824, 2007.

50. Tseng, W. J. and C. H. Wu, "Aggregation, Rheology and Electrophoretic Packing Structure of Aqueous Al_2O_3 Nanoparticle Suspensions", *Acta Materialia*, Vol. 50, No. 15, pp. 3757–3766, 2002.

51. Namburu, P. K., D. P. Kulkarni, D. Misra and D. K. Das, "Viscosity of Copper Oxide Nanoparticles Dispersed in Ethylene Glycol and Water Mixture", *Experimental Thermal and Fluid Science*, Vol. 32, No. 2, pp. 397–402, 2007.

52. Chen, H., Y. Ding, Y. He and C. Tan, "Rheological Behaviour of Ethylene Glycol Based Titania Nanofluids", *Chemical Physics Letters*, Vol. 444, No. 4–6, pp. 333–337, 2007.

53. Nguyen, C., F. Desgranges, N. Galanis, G. Roy, T. Maré, S. Boucher and H. Angue Mintsa, "Viscosity Data for Al_2O_3–water Nanofluid—hysteresis: Is Heat Transfer Enhancement Using Nanofluids Reliable?", *International Journal of Thermal Sciences*, Vol. 47, No. 2, pp. 103–111, 2008.

54. Einstein, A., "Eine Neue Bestimmung der Moleküldimensionen", *Annalen der Physik*, Vol. 324, No. 2, pp. 289–306, 1906.

55. Brinkman, H., "The Viscosity of Concentrated Suspensions and Solutions", *The Journal of Chemical Physics*, Vol. 20, p. 571, 1952.

56. Abu-Nada, E., "Effects of Variable Viscosity and Thermal Conductivity of Al_2O_3-water Nanofluid on Heat Transfer Enhancement in Natural Convection", *International Journal of Heat and Fluid Flow*, Vol. 30, No. 4, pp. 679–690, 2009.

57. Masoumi, N., N. Sohrabi and A. Behzadmehr, "A New Model for Calculating the Effective Viscosity of Nanofluids", *Journal of Physics D: Applied Physics*, Vol. 42, No. 5, 2009.

58. Batchelor, G., "The Effect of Brownian Motion on the Bulk Stress in a Suspension of Spherical Particles", *Journal of Fluid Mechanics*, Vol. 83, No. 1, pp. 97–117, 1977.

59. Koo, J. and C. Kleinstreuer, "A New Thermal Conductivity Model for Nanofluids", *Journal of Nanoparticle Research*, Vol. 6, No. 6, pp. 577–588, 2004.

60. Ahmad, T., P. SL and J. Myers, *FLUENT Theory Guide*, 13.0 edn., 2010.

61. Kundu, P., K. and I. Cohen, M., *Fluid Mechanics*, 4 edn, Elsevier, Oxford, 2008.

62. Hamilton, R. and O. Crosser, "Thermal Conductivity of Heterogeneous Two-component Systems", *Industrial & Engineering Chemistry Fundamentals*, Vol. 1, No. 3, pp. 187–191, 1962.

63. Chon, C. H., K. D. Kihm, S. P. Lee and S. U. Choi, "Empirical Correlation Finding the Role of Temperature and Particle Size for Nanofluid (AlO) Thermal Conductivity Enhancement", *Applied Physics Letters*, Vol. 87, 2005.

64. Manninen, M., V. Taivassalo and S. Kallio, *On the Mixture Model for Multiphase Flow*, Technical Research Centre of Finland, Finland, 1996.

65. Schiller, L. and A. Naumann, "A Drag Coefficient Correlation", *Vdi Zeitung*, Vol. 77, pp. 318–320, 1935.

66. Wang, C. Y. and C. Beckermann, "A Two-phase Mixture Model of Liquid-gas Flow and Heat Transfer in Capillary Porous Media-I. Formulation", *International Journal of Heat and Mass Transfer*, Vol. 36, pp. 2747–2747, 1993.

67. Syamlal, M. and D. Gidaspow, "Hydrodynamics of Fluidization: Prediction of Wall to Bed Heat Transfer Coefficients", *Aiche Journal*, Vol. 31, No. 1, pp. 127–135, 1985.

68. Bouillard, J., R. Lyczkowski and D. Gidaspow, "Porosity Distributions in a Fluidized-bed with an Immersed Obstacle", *Aiche Journal*, Vol. 35, No. 6, pp. 908–922, 1989.

69. Wakao, N. and S. Kagei, *Heat and Mass Transfer in Packed Beds*, Gordon and Breach, NewYork, 1930.

70. Kuipers, J., W. Prins and W. Van Swaaij, "Numerical-calculation of Wall-to-bed Heat-transfer Coefficients in Gas-fluidized Beds", *Aiche Journal*, Vol. 38, No. 7, pp. 1079–1091, 1992.

71. Shah, R. and A. London, *Laminar Flow Forced Convection in Ducts*, Academic Press, New York, NY, 1978.

72. Göktepe, S., K. Atalık and H. Ertürk, "Investigation of Single Phase Models for Predicting Pressure Drop in Nanofluid Flow in Circular Ducts", Accepted for IMECE 2013.

73. Göktepe, S., K. Atalık and H. Ertürk, "Comparative Analysis of Single and Two-phase Models for Nanofluid Forced Convection at the Entrance Region of a Uniformly Heated Tube", Under review for Internatioal Journal of Thermal Sceinces, 2013.

74. Munro, M., "Evaluated Material Properties for a Sintered alpha-Alumina", *Journal of the American Ceramic Society*, Vol. 80, No. 8, pp. 1919–1928, 1997.

75. Paszkowicz, W., J. Pelka, M. Knapp, T. Szyszko and S. Podsiadlo, "Lattice Parameters and Anisotropic Thermal Expansion of Hexagonal Boron Nitride in the 10–297.5 K Temperature Range", *Applied Physics A*, Vol. 75, No. 3, pp. 431–435, 2002.

76. Geick, R., C. H. Perry and G. Rupprecht, "Normal Modes in Hexagonal Boron Nitride", *Physical Review*, Vol. 146, pp. 543–547, 1966.

77. Oshima, C. and A. Nagashima, "Ultra-thin Epitaxial Films of Graphite and Hexagonal Boron Nitride on Solid Surfaces", *Journal of Physics: Condensed Matter*, Vol. 9, No. 1, p. 1, 1997.

78. "Boron Nitride Thermal Properties", 2001, http://www.ioffe.ru/SVA/NSM/Semicond/BN/thermal.html#Thermal%20conductivity, accessed at May 2013.